System Identification and Simulation of an Experimental Setup for Managed Pressure Drilling

Jussi Mikael Ånestad

June 10, 2013

Sammendrag

I denne masteroppgaven utvikles en simulator av en labrigg for eksperimenter relatert til heave-problematikk i MPD (Managed Pressure Drilling). Målet med laben er å utvikle kontrollmetoder for å undertrykke trykkforstyrrelsen som genereres av bølger. Simulatoren er basert på kvasilineære inkompressible 1D-rørstrømningslikninger, og implementeres ved å dekoble systemet og skrive om ved hjelp av Riemann-invarianter. Parametere knyttet til simulatoren diskuteres, og teoretiske resultater sammenliknes med eksperimentelle fra laben. Simulatoren finjusteres ved å tilpasse frekvensresponsen til nedhullstrykket. Det viser seg at lydfarten i simulatoren må justeres ned for å få resonanstopper på samme sted som på laben. Programmeringsspråket som brukes er C, som kjøres som C-MEX-funksjoner, for raskere kjøretider enn en ren MATLAB-implementasjon. Simulatoren oppfører seg tilfredsstillende for frekvenser opp til rundt 0.25Hz. Etter dette viser det seg at forenklingen ved å bruke sammenhengen for stasjonær strømning ikke holder. En distribuert observator implementeres i samme rammeverk og blir testet mot labdata. Her produserer den gode estimater for lav-frekvente forstyrrelser, men med noe fase-etterslep.

Abstract

This thesis looks at the development of a simulator for a lab setup related to heave-related issues in MPD (Managed Pressure Drilling) The aim of the lab is to create an environment for developing control methods to attenuate the pressure fluctuations generated by heave motion. The simulator is based on quasi-linear incompressible 1D pipe equations. The equations are simulated by decoupling and rewriting in terms of Riemann-invariants. The simulator parameters are discussed, and theoretical results are compared to experimental ones from the lab. The simulator is tuned by fitting the frequency response of the bottom hole pressure to the lab's. The wave speed of the simulator needs to be reduced significantly to align the resonance peaks with the frequencies found in experiments. Reasons for discrepancies between the lab and the model are discussed. The programming language used is C, through C-MEX functions for better runtimes. The simulator accuracy is satisfactory for disturbance frequencies up to about 0.25 Hz. For higher frequencies, the steady flow simplification used in the choke equation fails. A distributed observer is implemented within the same framework and is tested on data from the lab. The observer produces accurate estimates for low-frequency disturbances, but with a small phase lag.

Preface

This master's thesis was written the fall of 2013 as the final project in the M.Sc program for engineering cybernetics at NTNU, Trondheim. The project is a part of the work on creating a lab for simulating managed pressure drilling during heave motions of the drill string. Construction of the lab started in 2012 based on work by students from the Department of Petroleum Engineering and Applied Geophysics, and the building is very much still in progress, so some of the assumptions concerning the lab in this report are subject to change.

The work on the project has been inspiring and eye-opening. The dynamics of the relatively small-scale lab were (and some still are) mysterious and not easily modeled using textbook assumptions.

During the work on the lab, it was motivational and fruitful to have fellow students working on related problems. Thanks to Martin, Anders, Robert, Andreas and Anish for discussions and company during long days in the lab.

Long discussions and biweekly meetings with my supervisor Professor Ole Morten Aamo were invaluable for the progress with my project.

Down in the lab, Åge Sivertsen and Jarle Glad's presence and readiness has given us the opportunity to focus on our tasks by being gurus on the practical part of assembling the lab.

I would also like to thank my family and friends for being supportive, not only with this project, but throughout my whole education. Especially thanks to Katrine for helping me keeping my spirits up during the project work, and helping me making this report.

Jussi Mikael Ånestad
Trondheim, June 2013

Contents

List of Figures

List of Tables

Symbols and Abbreviations

Symbol	Explanation	Unit
c	Speed of sound	m/s
ρ	Density	kg/m^3
ρ_{ref}	The density of water at p_{ref}	kg/m^3
γ	Inclination angle (pipe inlet is the bottom)	rad
A	Copper pipe cross sectional area	m^2
u	Fluid velocity	m/s
g	Gravitational acceleration	m/s^2
U	Laplace transformed fluid velocity	
p	Pressure	Pa
q	Volumetric flow	m^3/s
p_c	Pressure at the choke inlet	Pa
p_0	Pressure at the choke outlet	Pa
P	Laplace transformed pressure	
u_c	Choke opening	[0..1]
q_c	Volumetric flow through the choke	m^3/s
q_b	Volumetric flow from the back pressure pump	m^3/s
G(u)	Choke characteristic function	
v_d	Piston velocity	m/s
V_d	Laplace-transformed piston velocity	
α	Upward-moving Riemann invariant	m/s
β	Downward-moving Riemann invariant	m/s

Table 0.0.1: *Frequently used symbols in the report*

Abbreviation	Explanation
MPD	Managed pressure drilling
BHA	Bottom hole assembly
BHP	Bottom hole pressure
NPT	Non-productive time
CBHP	Constant bottom hole pressure
MW	Mud weight
ECD	Equivalent circulation density
BP	Back pressure

Table 0.0.2: *Abbreviations used in the report*

Chapter 1 Problem Description

1. Collect all material that is relevant for modelling (project reports from IPT etc). Summarize all aspects of the lab that are relevant for mathematical modelling. Suggest how each component should be modelled, discussing assumptions and simplifications. Write the final complete mathematical model.

2. Implement the model in SIMULINK, starting from the preliminary simulator made last year.

3. List the parameters of the model and discuss their uncertainty. Devise algorithms/procedures for tuning parameters based on lab experiments. Carry out the procedures and implement them in the simulator.

4. Verify your simulator towards lab data.

5. Implement the distributed observer from [4] in the same framework as the simulator, and test it on lab data.

6. Document the code.

7. Write a report.

Chapter 2 Introduction

The worldwide demand for energy is increasing as emerging markets get industrialized. At the same time drilling operations are getting more and more challenging as reservoirs get depleted, and we're left with the seemingly undrillable prospects.

One of the main challenges that has to be met is drilling when the pressure window between collapse and fracture pressures is narrow.

With conventional drilling techniques, the downhole pressure is controlled by varying the pump rate and the density of the mud that is pumped down through the drill string, but this method has limitations when it comes to precision and bandwidth. During static conditions, such as connections and trips, we are relying on the hydrostatic pressure.

Deviations from the required wellbore pressure can cause big problems. If the pressure is too high, the formation might fracture, and we get a loss of circulation in the well, and if it's too low, we risk getting an influx (kick). In either case the drill pipe might get stuck, and even worse, a blowout may occur, potentially resulting in equipment damage and loss of lives.

With conventional drilling, cement and various LCMs (loss of circulation material) have typically been used to repair the well, but this does only last for a while, resulting in more cement and delays. Examples where cement has been pumped in excess of 30 times on a single well are common [26].

Managed pressure drilling (MPD) is a way of preventing these potentially hazardous events from happening, by giving the driller the ability to control the downhole pressure precisely.

MPD both leads to more predictable costs for the driller, and a safer, more environmentally friendly world for everyone else.

In this thesis, we will firstly review MPD, and then look at the IPT Heave lab, a lab designed to explore control methods for MPD use. The main part of this text will deal with a mathematical model and a simulator of this lab.

Chapter 3 Managed Pressure Drilling

This chapter is based on an introduction to MPD from the fall 2012 report [27].

MPD is not just one technique, but rather a class of different drilling techniques with some properties in common. MPD techniques usually differ from conventional ones in mainly two ways [13]:

- Mud does not return to surface at atmospheric conditions (zero back pressure)
- Mud is circulated not just using energy supplied by drill pipe injection

To illustrate the convenience of the first property, look at the pressure profile in figure 3.0.1. The dotted lines show the pressure in the well during static conditions. The conventional well relies on just the hydrostatic pressure, and has to use a heavier mud to maintain the same pressure as the MPD well, where a lighter mud is used accompanied by back pressure from a choke manifold on the top of the well to give the pressure profile an offset.

Another feature MPD techniques have in common, is the use of a rotating control device (RCD) to seal the top of the annulus. All MPD techniques also maintain the pressure in the well balanced or overbalanced.

3.1 Different MPD Techniques

The various MPD techniques are categorized as either reactive MPD, or proactive MPD by IADC.

Reactive MPD techniques are used in wells designed for conventional drilling to be able to react to kicks and avoid unwanted discharges for HSE reasons. Reactive MPD techniques also use an RCD, but the equipment is not brought into play unless unexpected changes in the downhole pressure occur.

Proactive MPD is MPD used in wells planned especially for MPD drilling, where the equipment is actively used to control the annular pressure profile. The reactive option has been implemented for years, but the proactive ones have not been applied much until recently [25].

The main focus of this project is the MPD method known as constant bottom hole pressure.

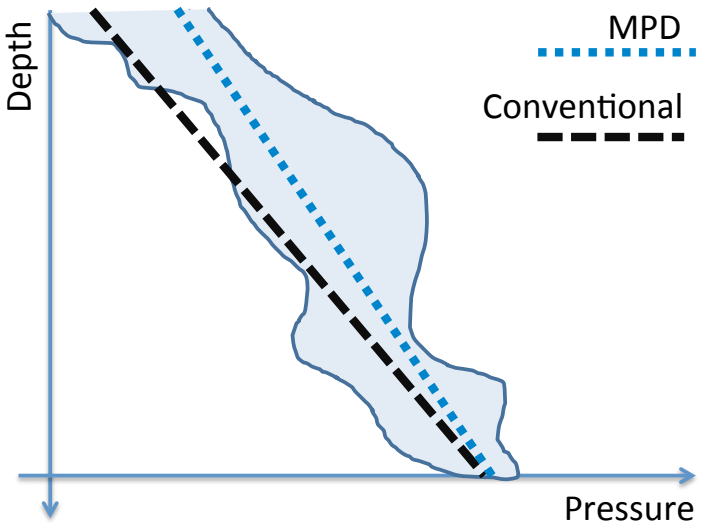

Figure 3.0.1: *Pressure profile. The blue area depicts the drilling window we have to stay within. During static conditions, the pressure gradient in the conventional well is only the hydrostatic pressure, while in the MPD well it consists of the hydrostatic pressure and a back pressure from a choke and possibly a dedicated back pressure pump.*

3.1.1 CBHP (Constant Bottomhole Pressure)

The goal in the constant bottom hole pressure variant of MPD is to maintain a constant annulus pressure profile. This is important in wells with a narrow pressure window, to avoid kick-loss cycles. When the main pumps are turned off in a conventional well, the equivalent mud weight (EMW) is reduced to the hydrostatic pressure of the mud. If the pressure window is narrow, this drop might cause an influx (kick). When the pumps start again, the EMW increases, which might cause fluid losses into formation [2].

The pressure profile is kept nearly constant by applying a back pressure with a choke. The choke may also be supplemented by a back pressure pump at the top of the well. See figure 3.0.1 for an illustration of the added degree of freedom supplied by this method.

	Conventional drilling	CBHP MPD drilling
BHP during drilling	MW + ECD	MW + ECD + BP
BHP when not drilling	MW	MW + BP

Table 3.1.1: *Bottom hole pressure (BHP) comparison, conventional drilling versus CBHP drilling. MW is the mud weight, ECD is the equivalent circulation density which is a function of pump rate and mud rheology and BP is the back pressure provided by the choke (and optionally a back pressure pump).*

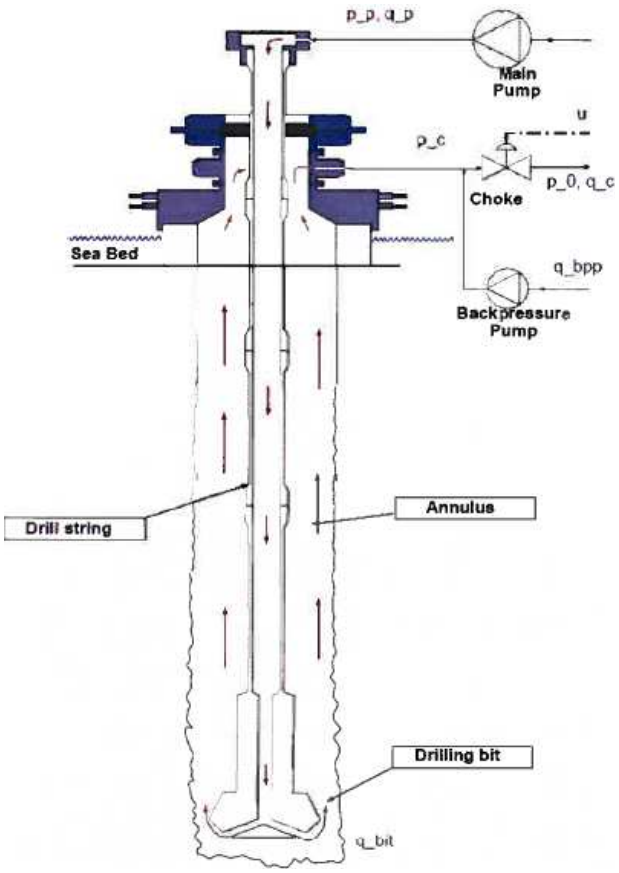

Figure 3.1.1: *Schematics for a CBHP MPD rig with a dedicated backpressure pump [18].*

3.2 Automation of MPD

There are both automated and manually controlled versions of MPD. The manual version requires a trained choke operator to adjust the back pressure manually. This works when the pressure window is not too narrow. By manually controlling the choke opening, the MPD operators at Gullfaks C managed to keep the pressure within ± 5 bar for most operations in the well C09A, but in the well C01A, the pressure windows were sometimes as narrow as ± 2.5 bar, and automated MPD was necessary [17].

The control system adjusts the choke to maintain a desired BHP. The BHP can be measured directly with a measurement while drilling (MWD) tool, which transmits measurements to surface by a telemetry pipe or by mud pulse telemetry. Mud pulse telemetry is the most common solution, but has a low bandwidth, typically 0.03Hz. This information is used to monitor and predict the annular pressure, and calculate the setpoint to be sent to the choke's programmable logic controller (PLC).

Many major oil companies have developed automated MPD systems. Statoil has been developing one the last 3-4 years. Their system consists of two main components: a downhole pressure estimator, and a choke pressure controller. Both of the components are nonlinear, and are based on a simple hydraulic model with 3 states (main pump pressure, upstream

choke pressure, flow through the drilling bit). The control strategy is to use the desired choke pressure, and the derivative of the desired choke pressure to calculate a desired flow through the choke, which corresponds to a choke opening by using the choke characteristic. The desired choke pressure is calculated by using the relation from 3.1.1, where the ECD pressure contribution (friction) is estimated based on topside measurements. This control system has been successfully tested on a full scale drilling rig [18].

The whole control system is sometimes called a dynamic annular pressure control (DAPC) [12].

3.3 Challenges

This section covers some of the main challenges related to controlling the BHP stable in offshore wells.

3.3.1 Surge and Swab Pressures

Vertical motion of the drill string is inevitable during drilling. The drill bit becomes worn after a while, and has to be replaced. This requires the drill string to be pulled out, and ran back in. Connections do also require the drill string to be lifted. Even though drilling operators have to abide a maximum safe trip speed, all these motions create pressure changes in the wellbore, and the piston effect may pose a problem if the pressure window is narrow. This is especially a problem when the annular clearance is low and/or the mud volume is low. [8]

3.3.2 Heave Motion on Floating Rigs

Floating rigs are used in the exploratory phase of drilling or when drilling in deep waters (more than 500 m). Maintaining a constant BHP from a floating rig is even harder than from a fixed platform, because of heave motion from the rig. In the North Sea, there is especially rough sea during fall and winter, which can potentially put drilling operations on hold for several days. The heave motion can be attenuated by the rig's heave compensator during drilling and tripping, but during connections, when new segments are added to the drill string, the drill string moves up and down with the heave of the rig. An alternative that reduces the BHP-control requirements is to use a heave-compensated drill floor. [8]

3.3.3 Time Delay

From a control point of view, the time delay imposed by the distance between the choke and the bottom of the well makes the control of the BHP challenging. The length of the drill string also poses problems when it comes to predicting the effect of the heave disturbance. When the length of the drillstring is in the order of kilometers it acts more like a rubber band than a stiff steel pipe. A good hydraulic model for the well, and a predictive algorithm is crucial to be able to counteract heave motion before it is too late.

3.4 Applications Today and in the Future

MPD has a long tradition in land applications. Based on a survey by Weatherford, more than 60% of US land programs drill at least one section with some form of MPD. NPT is significantly more costly offshore, MPD is thus thought to have an even bigger potential for offshore drilling programs than for the land drilling programs that developed the technique [19].

A survey was done where offshore technology users and providers were asked what percentage of all offshore wells they though would apply MPD 5 years from now (the survey was conducted in 2011), given that steps were taken to accelerate the industry acceptance. The respondents indicated that 40% of all offshore wells will use MPD in 2015. One service provider predicted that the biggest potential for offshore MPD lies in the floating drilling market [20].

MPD methods in use today largely focus on control of backpressure, but methods that can manipulate other parameters like fluid density, rheology, annular fluid level, circulating friction and hole geometry are being developed [14].

Chapter 4 The MPD Heave Rig

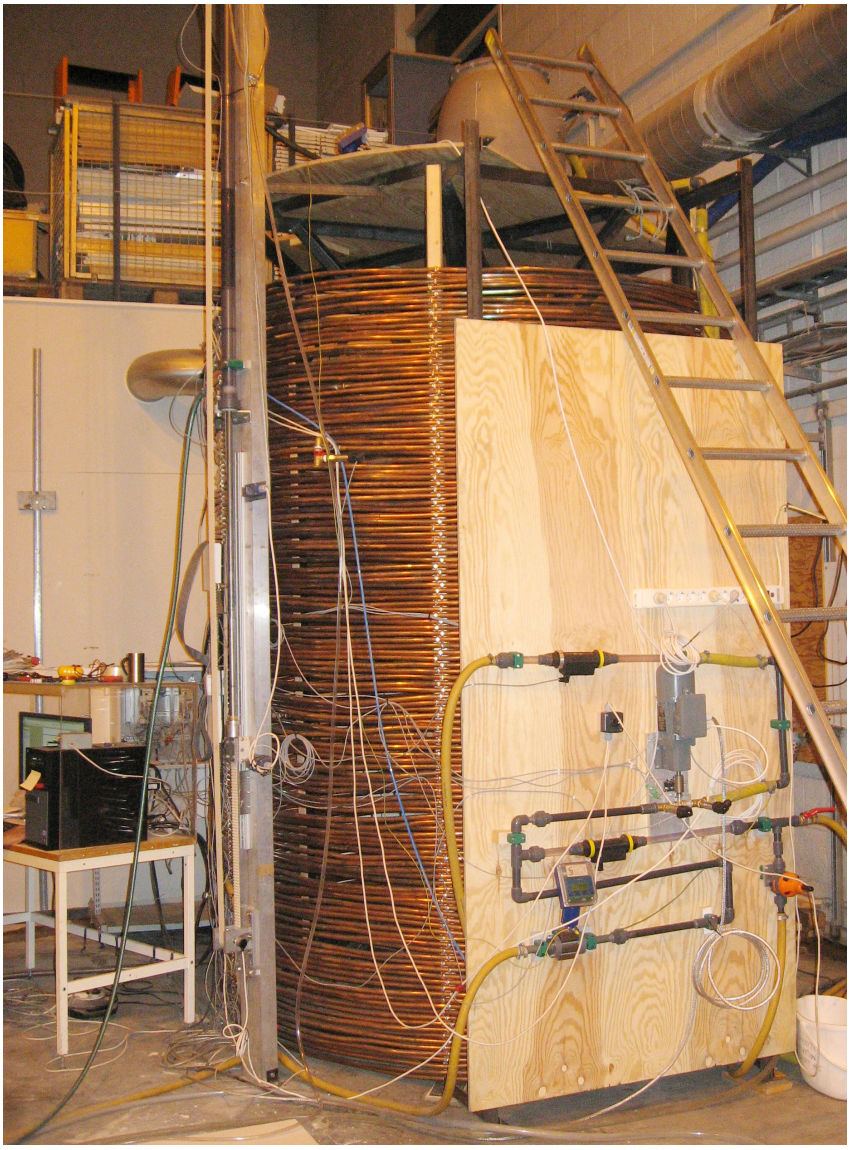

Figure 4.0.1: *The Rig*

The planning of the MPD heave rig started the fall of 2011, when three master's students from the Department of Petroleum Engineering & Applied Geophysics were working with a

model for the lab. Two project reports were submitted; Gjengseth and Svenum (2011) and Rashid (2011). These mainly address the physical design of the lab rig, and do not look at control system designs. Later, two master's theses by Svenum (2012) and Gjengseth (2012) were submitted, with a larger focus on mathematical modeling of various pressure drops in the system.

The MPD heave rig planning was based on data from a 4000 m deep vertical well where a drill string with a diameter of 5" is in a 8.5" diameter hole with a BHA (Bottom Hole Assembly) of 70 m, and is exposed to heave with an amplitude of 1.5 meters and a period of 11 seconds. The drill string consists of a drill collar and a drill bit with a diameter of 6.5". A choke opening on the surface, 4000 meters above the bottom, compensates pressure variations downhole.

To include the time delay implied by having the choke opening 4000 meters above the bottom, a 900 m long copper pipe is used.

4.1 Components

4.1.1 Backpressure

A backpressure loop continuously circulates water from a water tank at a rate of approximately 28 lpm. A pump provides the flow, and a choke is used to adjust the backpressure.

The pump is a C980A Hawk pump which theoretically can deliver 140 bar at a flow rate 40 lpm (10,6 kW) at 1450 rpm and or 47.3 l/min (12.5 kW) at 1740 rpm. The pump is controlled manually with a frequency converter where the rate can be set to 0-100%. However, the pump turned out to only deliver about 30 lpm. To remedy this, a feed pump was installed. This has as far as the author can tell not improved the flow rate significantly, and the maximum flow rate is still about 30 lpm.

An unresolved problem with the back pressure pump is that noise (either vibrations or electromagnetic) propagates to the pressure sensors on the copper pipe whenever it is running. As of the spring 2013, the solution to this has been either using the pressurized tank instead of the pump whenever this is a possibility, or low-pass filtering the pressure data.

The choke valve is a tailored system consisting of a 90 degree 1/2" ball valve driven by to a three-phase AC motor supplied by Lenze. A new valve was installed the spring 2013 due to a backlash problem discovered the fall of 2012.

4.1.2 Sensors

The differential pressure over the choke is measured by two pressure transmitters placed on either side of the choke (C1 downstream, C2 upstream), and the flow rate is measured by three flow meters (FT3 downstream the choke, FT2 on the pump outlet, FT1 on the copper pipe outlet). A pressure transmitter is used to measure the water level in the tank.

There are also pressure transmitters every 100th meter of the copper piping (PT1-PT10), where PT1 is on floor level, and two pressure transmitters are in the heave generator (P1

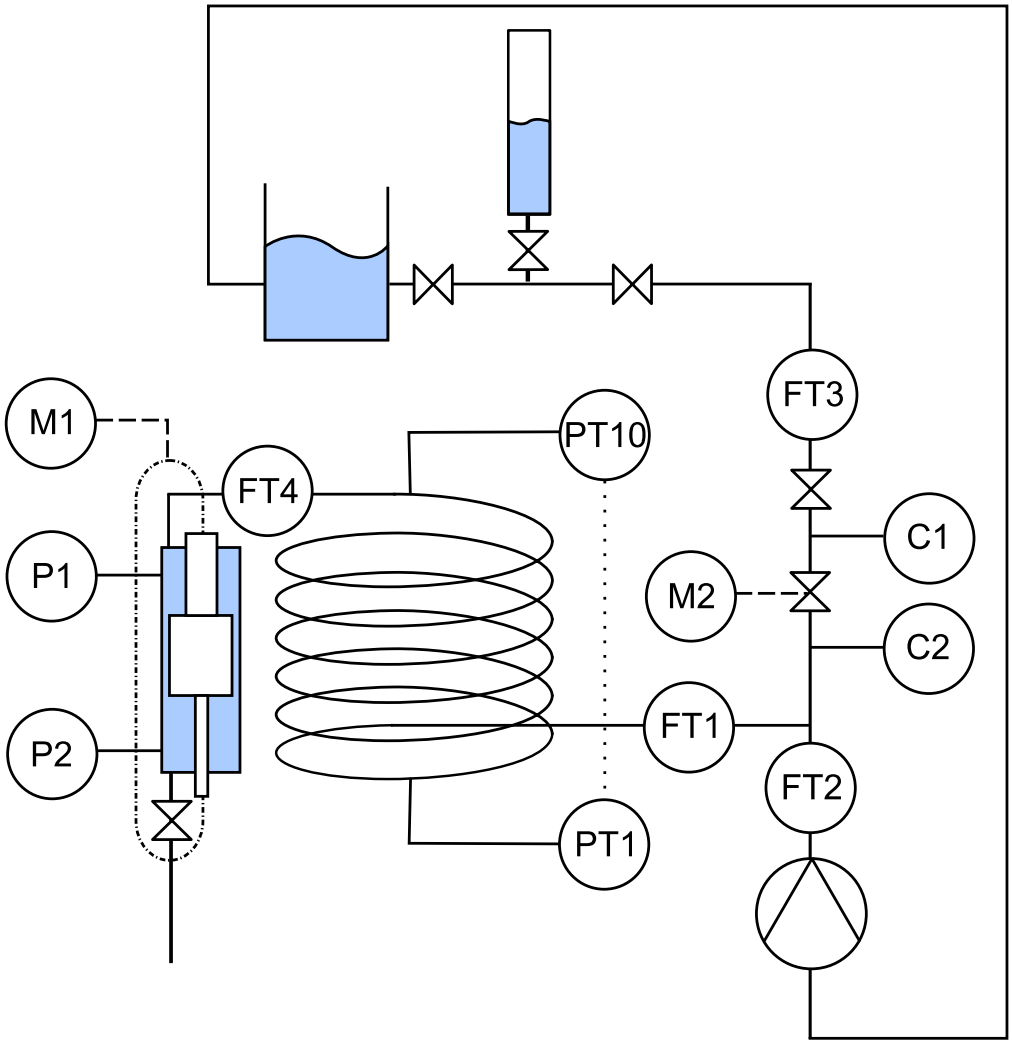

Figure 4.1.1: *A sketch of the MPD Heave Rig. Note that not all sensors and valves are depicted. For example, there is a bypass line for the copper pipe enabled by remotely controlled valves.*

Parker DFT990	Heinrichs EP/UMF2	UNIK 5000 PS	PTX 1400
			
Turbine flow meter	Magnetic flow meter	Pressure transmitter	Pressure transmitter
Accuracy: ±2%	**Accuracy:** ±0.3%	**Accuracy:** ±0.15%	**Accuracy:** ±0.15%
Output: 4-20 mA	**Output:** 4-20 mA	**Output:** 4-20 mA	**Output:** 4-20 mA
Range: 4-100 l/min	**Range:** 0.5-10 m/s	**Range:** 0-16 bar	**Range:** 0-100 mbar

Table 4.1.1: *The sensors used in the lab rig*

on floor level, P2 on the top), and a flow meter is on the inlet of the copper piping (FT4) is due to be installed within the fall of 2013.

Note that as of May 2013, FT1 is the only bidirectional flow meter in the lab.

4.1.3 DAQ Board

The 4-20 mA signals from the sensors are converted to 2-10 V signals by connecting the current signals to resistors on an analog termination board. Flat cables with the voltage signals are ran from the termination board to two National Instruments SCB-68 connector blocks, and transmitted with two SCSI cables to a NI PCI-6289 DAQ-board.

Output signals to control the choke and heave generator are transmitted from the computer to SCB-68 connector block A with one of the two SCSI cables, then via two wires to two 8400 Topline frequency inverters, which are connected to the motors.

4.1.4 Heave Generator/Piston

To generate the heave disturbance, a motor is connected to a wheel with a toothed belt, which is attached to a BHA moving up and down in a closed compartment to simulate the heave disturbance. During the modeling process, many different BHA diameters have been considered, and the current one might be subject to change to achieve the wanted disturbance. Work was done during the fall 2012 by Martin Standal Gleditsch [16] and Robert Tafjord Drønnen [9] to enable use of more arbitrary reference signals, and improved further the spring of 2013 by Robert Tafjord Drønnen and Anders Albert.

4.1.5 Pressurized Tube

A vertical tube with water and pressurized air was installed the spring of 2013 downstream the choke (as an alternative to the open tank) to enable a stable pressure higher than atmospheric pressure. This may be used as an alternative to the back pressure pump to avoid making a vacuum in the system when the heave generator is active.

4.1.6 Simulink I/O

The Real-Time Windows Target is used for all I/O handling. In the absence of information about which sensors are connected to which channel on the PCI board, the input channels were identified by looking at scopes in Simulink while disconnecting sensors. This was done in collaboration with Martin Standahl Gleditsch [16]. The final channel list, and corresponding sensor types can be seen in table C.0.1. The I/O channels may be found in appendix C.

4.2 Changes from Last Year

4.2.1 Bidirectional Flow Meters

The FT1 flow meter was replaced due to problems, and the fact that it did not transmit any sign information to the computer, which is necessary since the flow in the copper pipe is oscillating about zero flow. The new flow meter is a Heinrichs Magnetic Inductive Flow Meter with an UMF2 transmitter. The sign information is given as the output signal on a dedicated status output port. Notably, the signal is passive, transmitted via an optocoupler, so an external voltage source was installed to get the readings. The sign bit is high (6V) for reverse flow.

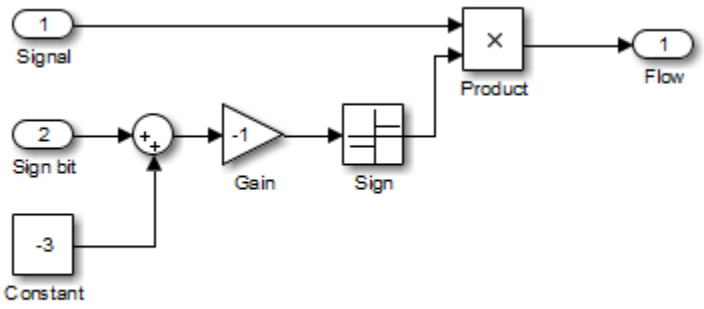

Figure 4.2.1: *Simulink implementation of sign information.*

4.2.2 Calibration of the New Flow Meter

An experiment was done to determine the scaling factor needed to get the FT1 data in liters/minute. Water was ran from the pump with the choke valve closed (a manual valve next to the choke installed this year to enable complete blockage of the choke flow), and the valve under the piston open. The flow was measured by filling up a bucket and writing down the weight of the bucket every 10 seconds. This experiment was done 3 times, with different flows from the pump, and resulted in the scaling in table 1. The biases were found by averaging the sensor readings before the pump was turned on. FT2 and FT3 had the same scaling factors last year.

Pump flow	FT1 [lpm]	FT2 [lpm]
30%	1.1897 · (FT1-2)	0.9653 · (FT2-2)
40%	1.1835· (FT1-2)	0.9196· (FT2-2)
50%	1.1895· (FT1-2)	0.9050· (FT2-2)
Mean	1.1875· (FT1-2)	0.9300· (FT2-2)

Table 4.2.1: *Flow meter scaling factors*

Chapter 5 Mathematical Modeling

5.1 Previous Modeling Work

Modeling work related to the IPT heave lab has previously been done by Svenum [29], Boge [6] and Gjengseth [15] from the Department of Petroleum Engineering and Applied Geophysics. This has mostly been static considerations not directly applicable to the simulator, but nonetheless, a very brief summary follows.

5.1.1 Choke

The choke has been modeled with the steady choke equation, where the flow is the product of the square of the differential pressure and a characteristic function, and the choke characteristic has been determined in several reports, including [27]. In addition, a large backlash was identified. However, the choke has been replaced, and a new identification is necessary.

5.1.2 Piston

The losses over the BHA have been theoretically calculated, as a sum of the following contributions [6, 29]

- Friction
- Entrance loss
- Exit loss
- Acceleration of the lower rod
- Acceleration of the upper rod
- Hydrostatic pressure

The final mathematical expression is a function of the piston acceleration, piston position, mean fluid velocity (which is modeled in terms of the piston velocity and a clinging factor parameter) as well as the physical dimensions of the piston compartment. In addition, a linear relation for the pressure drop as a function of the piston velocity has been showing promising results.

5.1.3 Pipe friction

The friction in the pipe has been calculated theoretically, using a steady, laminar flow assumption and the Fanning friction factor. In addition,[29] has also accounted for the curvature of the pipe, obtaining a ratio $f_{coiled}/f_{straight}$of 1.65 for a given Reynolds number.

5.1.4 Dynamics

[16] identified a larger time delay in the system than expected.

A simulator of the lab was made last year [3] in MATLAB/Simulink. This simulator, however, has not been verified on lab data. This report will use that simulator as a basis.

5.2 Flow in the Copper Pipe

The flow in the copper pipe is modeled as inviscid one-dimensional flow with quadratic friction. The relationship between pressure and density used is [28]

$$\rho(t,x) = \rho_{ref} + \frac{p(t,x) - p_{ref}}{c^2} \tag{5.2.1}$$

where c is the speed of sound, and ρ_{ref} is the reference density at reference pressure p_{ref}. This is the definition of the speed of sound linearized: $c^2 = (\frac{\partial p}{\partial \rho})_s$. The equation of continuity, when radial and angular dynamics are neglected is

$$\frac{\partial \rho}{\partial t} + \frac{\partial}{\partial x}(\rho u) = 0$$

and when (5.2.1) is inserted, this can be rewritten as:

$$\frac{\partial p}{\partial t} + (p+k)\frac{\partial u}{\partial x} + \frac{\partial p}{\partial x}u \;\; = \;\; 0 \tag{5.2.2}$$

Since the fluid velocity in the pipe is significantly lower than the speed of sound, we will use the Navier-Stokes-equation for incompressible fluid, which when radial and angular dynamics are neglected, and a lumped friction acceleration term is added, can be written:

$$\frac{\partial u}{\partial t} + u\frac{\partial u}{\partial x} + \frac{1}{\rho}\frac{\partial p}{\partial x} + g\sin(\gamma) + f(u) = 0$$

By defining

$$k = c^2\rho_{ref} - p_{ref}$$

we can write:

$$\frac{\partial u}{\partial t} + u\frac{\partial u}{\partial x} + \frac{c^2}{k+p}\frac{\partial p}{\partial x} + g\sin(\gamma) + f(u) \;\; = \;\; 0 \tag{5.2.3}$$

The boundary conditions chosen for the model are:

$$u(t,0) = u_0(t) \tag{5.2.4}$$
$$p(t,l) = p_l(t) \tag{5.2.5}$$

5.3 Choke

The flow through the choke is assumed to be the sum of the flow from a back pressure pump and from the pipe:

$$q_c = q_b + q_w \tag{5.3.1}$$

where q_b is a constant parameter and $q_w = Au(l,t)$, where A is the cross-sectional area of the pipe. We will assume that $q_c \geq 0$ at all times, and that the back pressure pump is controlled so that this is assured. A formula that valve manufactureres often cite for liquid volume rate through a valve is

$$q_c = G(u_c)\sqrt{\frac{1}{\rho_L}(p_c - p_0)} \tag{5.3.2}$$

Where $G(u_c)$ is the flow coefficient as a function of the choke opening, also known as the choke characteristic, and p_c and p_0 are the pressures at the choke inlet and outlet respectively. The outlet pressure is a constant parameter.

The dynamics of the choke are modeled as a first order filter with a saturated angle rate.

An alternative model to the static choke equation is the dynamic orifice equation [1]

$$b_1\frac{\partial q_c}{\partial t} + b_2 q_c^2 = \frac{p_c - p_0}{\rho} \tag{5.3.3}$$

where b_1 and $b_2$are functions of the choke opening. This equation reduces to 5.3.2 for steady flows.

Regardless of the model choice, getting a perfect fit for all disturbance frequencies and flows is unlikely, due to the different physical properties of different flow regimes, and our 1D simplification.

5.4 Piston

The piston is representing the bottom hole assembly moving vertically.

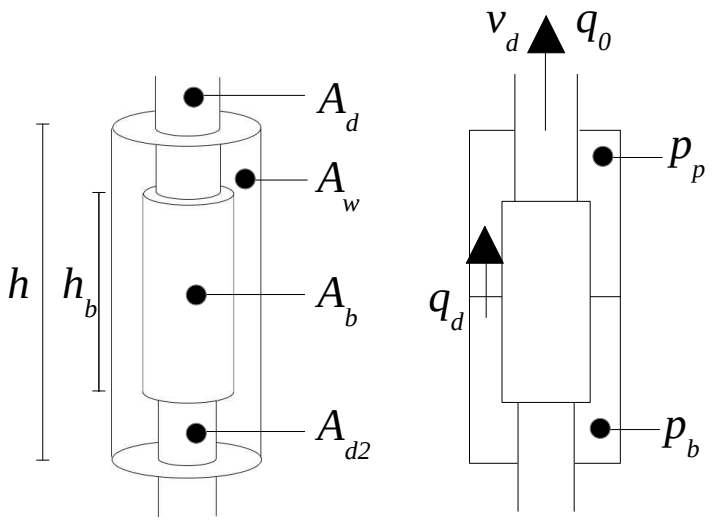

Figure 5.4.1: *Quantities in the piston model. The piston compartment has cross-sectional area A_w and height h. The bottom hole assembly is represented by a piston that moves vertically with velocity v_d. The piston has cross-sectional area A_d and height h_b. At its upper side, the piston is connected to the drill string, which has cross-sectional area A_{d2}. The pressures in the control volumes above and below the piston are denoted by p_p and p_b respectively. q_d is the flow of displaced fluid between them and $q_0$is the flow into the copper pipe.*

It is modeled by the following equations

$$q_0 = -v_d(A_d - A_{d2}) \tag{5.4.1}$$
$$p_b - p_p = f_{d,1} \cdot v_d + f_{d,2} \cdot v_d \cdot |v_d| + \rho g h = \Delta p_f + \Delta p_g \tag{5.4.2}$$

5.4.1 Previous Model

The piston was formerly modeled as two control volumes and three states, one for the pressure in each of the control volumes, and one for the flow between them, as follows

$$\dot{p}_p = \frac{\beta_p}{V_p}(q_d - q_0 + v_d(A_b - A_d)) \tag{5.4.3}$$
$$\dot{p}_b = \frac{\beta}{V_b}(-q_d - v_d(A_b - A_{d2})) \tag{5.4.4}$$
$$\dot{q}_d = \frac{1}{M}(p_b - p_p - \Delta p_f - \rho g h) \tag{5.4.5}$$

Where Δp_f is the pressure drop due to friction. This model was abondoned for several reasons. Mainly, because its contribution to the dynamics were practically exactly the same as 5.4.1 (the resulting pipe inlet flow was identical), while slowing down the runtimes of the

simulator (and even causing problems with some solvers). Secondly, because it was hard to identify the parameters due to the lack of a flow meter (FT4). Source code for a version of the simulator with this model implemented is enclosed.

Chapter 6 Implementation

6.1 Solution Method

6.1.1 Grid Types

To simulate a PDE, there are several discretization methods. Some use a collocated grid, which means that the pressure and velocity information is stored in the same nodes. However, since we do not know the direction of the flow in every point, we have to use a central-difference approach to calculate the derivatives. This is known to cause an odd-even-decoupling of the system. That is, the gradient in odd-numbered nodes only uses information from even-numbered nodes, and vice-versa. A remedy for this is to use a staggered grid, where the pressure values are stored in cell centers of the control volumes, while the velocity variables are stored at the cell faces [11].

6.1.2 Upwind Scheme

A different approach is to decompose the system to separate the information moving in the positive x-direction from that moving in the negative x-direction, and then use a forward-difference approach for the forward moving part, and a backward-difference method for the backwards moving part. This principle is known as the upwind scheme. (upwind scheme principle, [11]. This is the approach chosen for the MPD rig simulator. The decomposition of the system is done by a diagonalizing change of variables. See B.2 for an outline of the method.

To decompose our system (5.2.3) and (5.2.2), we start by writing the system in matrix notation $\mathbf{z_t} + \mathbf{A}(\mathbf{z})\mathbf{z_x} = \mathbf{0}$ (indices denoting partial derivatives). We will ignore the friction and gravity terms for now.

$$\mathbf{z} = \begin{bmatrix} p & u \end{bmatrix}^{\mathbf{T}}$$

$$\mathbf{A}(\mathbf{z}) = \begin{bmatrix} u & k+p \\ \frac{c^2}{k+p} & u \end{bmatrix} \tag{6.1.1}$$

The matrix $\mathbf{A}(\mathbf{z})$ has the characteristic equation

$$\lambda^2 - 2u\lambda + (u^2 - c^2) = 0$$

Which results in the eigenvalues

$$\lambda^{(1,2)} = u \pm c \tag{6.1.2}$$

And the corresponding left eigenvectors

$$\mathbf{l}^{(1,2)} = \begin{bmatrix} \frac{\pm c}{k+p} & 1 \end{bmatrix} \tag{6.1.3}$$

The Riemann invariants are defined by

$$\alpha(p,u) = \int l_1^{(1)} dp + \int l_2^{(1)} du \tag{6.1.4}$$

$$\beta(p,u) = \int l_1^{(2)} dp + \int l_2^{(2)} du \tag{6.1.5}$$

When integrated, we get the two invariants

$$\alpha(p,u) = c\ln(k+p) + u + K_1 \tag{6.1.6}$$

$$\beta(p,u) = -c\ln(k+p) + u + K_2 \tag{6.1.7}$$

The integration constants K_1 and K_2 are chosen such that when $\alpha = \beta = 0$, we have $p = \overline{p}$ and $u = \overline{u}$, where $\bar{p}$ and $\bar{u}$ are arbitrary constants. This leads us to the new coordinates

$$\alpha(p,u) = c\ln(\frac{k+p}{k+\bar{p}}) + u - \bar{u} \tag{6.1.8}$$

$$\beta(p,u) = -c\ln(\frac{k+p}{k+\bar{p}}) + u - \bar{u} \tag{6.1.9}$$

Differentiating (6.1.8) and (6.1.9) leads us to the differential equations

$$\alpha_t = c\frac{p_t}{k+p} + u_t \tag{6.1.10}$$

$$\beta_t = -c\frac{p_t}{k+p} + u_t \tag{6.1.11}$$

We can rewrite the equations in terms of α and β by using the inverse of (6.1.8) and (6.1.9)

$$p(\alpha,\beta) = (k+\bar{p})\exp((\alpha-\beta)/(2c)) - k \tag{6.1.12}$$

$$u(\alpha,\beta) = \bar{u} + (\alpha+\beta)/2 \tag{6.1.13}$$

Inserting p_t and u_t from (5.2.2)-(5.2.3) into (6.1.10)-(6.1.11) gives

$$\alpha_t = -c\frac{up_x + (k+p)u_x}{k+p} - uu_x - \frac{c^2}{k+p}p_x - g\sin(\gamma) - f(u) \tag{6.1.14}$$

$$\beta_t = c\frac{up_x + (k+p)u_x}{k+p} - uu_x - \frac{c^2}{k+p}p_x - g\sin(\gamma) - f(u) \tag{6.1.15}$$

Insering p and u from (6.1.12)-(6.1.13) gives

$$\alpha_t = (-c - \bar{u} - \frac{\alpha+\beta}{2})\alpha_x - g\sin(\gamma) - f(\bar{u} + \frac{\alpha+\beta}{2}) \tag{6.1.16}$$

$$\beta_t = (c - \bar{u} - \frac{\alpha+\beta}{2})\beta_x - g\sin(\gamma) - f(\bar{u} + \frac{\alpha+\beta}{2}) \tag{6.1.17}$$

6.2 Programming Language

The preliminary simulator was implemented as a .m s-function prior to this project. However, the run times were considered too high for the simulator to be useful for real-time purposes. It was decided to translate the .m s-function into a C MEX s-function. This turned out to make the simulator significantly faster, see 7.4 for the result of a comparison.

6.3 Data Structure

The MATLAB S-function keeps track of a state vector. The states of the lab simulator are the values of the Riemann-invariants for every discretization element (the number of elements, N, can be changed in the source code A.5). The state vector is shown in table 6.3.1.

State	$\alpha(0)$	$\cdots$	$\alpha(N-1)$	$\beta(0)$	$\cdots$	$\beta(N-1)$	u
Variable	x[0]	$\cdots$	x[N-1]	x[N]	$\cdots$	x[2N-1]	x[2N]

Table 6.3.1: *State vector in the S-function*

In table 6.3.2, the state variables corresponding to each spatial discretization element is shown. Notice that the data for the α- and β-elements are shifted by one cell.

Spatial coordinate	$x = 0$	$x = \frac{L}{N}$	$x = 2\frac{L}{N}$	$\cdots$	$x = (N-1)\frac{L}{N}$	$x = L$
C variable name	alphaStart	x[0]	x[1]	$\cdots$	x[N-2]	x[N-1]
Contents	α_{start}	$\alpha(0)$	$\alpha(1)$	$\cdots$	$\alpha(N-2)$	$\alpha(N-1)$
C variable name	x[N]	x[N+1]	x[N+2]	$\cdots$	x[2N-1]	betaStart
Contents	$\beta(0)$	$\beta(1)$	$\beta(2)$	$\cdots$	$\beta(N-1)$	β_{start}

Table 6.3.2: *Data structure*

6.4 System Parameters

The parameters of the simulator and their C constant names are shown in table 6.4.1. The constants are specified in the mask parameters dialog and may be changed by double-clicking on the simulator block.

Parameter name	C constant name	Description
CS area of pipe	C_A	The cross-sectional area of the pipe [m^2]
Reference pressure	C_P_REF	The reference pressure in 5.2.1
Reference density	C_RHO_REF	The reference density in 5.2.1
Linear pipe friction	C_F1	The linear friction coefficient discussed in 8.6
Speed of sound	C_F2	The quadratic friction coefficient discussed in 8.6
Pbar	C_PBAR	The constant from 6.1.2
Ubar	C_UBAR	The constant from 6.1.2
Pressure at outlet	C_P_OUT	The pressure at the choke outlet (C1) [Pa]
Initial pressure at choke	C_PL	The initial pressure at the choke (C2) [Pa]
Choke closing time	C_T	The choke time constant [s]
Choke fluid density	C_CH_RHO_L	The fluid density at the choke [kg/m^3]
Inclination angle	C_GAMMA	Inclination angle from pipe inlet (bottom) to choke (top) (rad)
Piston compartment height	C_CH	The height of the piston compartment [m]
CS area of drill string	C_CAD	The cross-sectional area of the upper rod [m^2]
CS area of drill string below piston	C_CAD2	The cross-sectional area of the lower rod [m^2]
Piston linear friction	C_CF1	The linear friction coefficient discussed in 8.2
Piston quadratic friction	C_CF2	The quadratic friction coefficient discussed in 8.2
Length of pipe	C_L	The length of the copper pipe [m]
Desired pressure outputs	C_K	A vector of the x-positions of the desired pressure outputs [m]
Choke characteristic	C_G	A vector of evenly spaced choke characteristic values
Piston height	C_CHB	The height of the BHA [m]
CS Area of piston	C_CAB	The cross-sectional area of the BHA [m^2]
CS Area of comp	C_CAW	The cross-sectional area of the piston compartment [m^2]
Bulk modulus	C_BETA	The bulk modulus in the piston compartment. [Pa]
Static outputs	C_STATIC_OUTPUTS	The number of outputs not including the customizable ones

Table 6.4.1: *Simulator parameters*

6.5 Initialization

The initial condition of the model is given by the steady state solution resulting from zero flow at the pipe inlet, and a pressure equal to p_l at the outlet (given as a parameter). The steady state solution $\bar{p}(x)$ calculated from 5.2.3 must then satisfy

$$\frac{c^2}{k+\bar{p}}\frac{\partial \bar{p}}{\partial x} + g\sin(\gamma) = 0 \tag{6.5.1}$$

Integrating with respect to x yields

$$\ln(k+p_l) - \ln(k+p_l)\exp(\frac{g}{c^2}\int_x^l \sin(\gamma)\,dz) = 0 \tag{6.5.2}$$

As the inclination γ is constant in the copper pipe, this can be simplified to

$$\bar{p}(x) = (k+p_l)\exp(\frac{g}{c^2}(l-x)\sin(\gamma)) - k \tag{6.5.3}$$

The initial choke opening is set to match p_l and the initial back pressure pump flow, that is

$$u_c = G^{-1}\left(\sqrt{\frac{\rho_L q_b^2}{p_l - p_0}}\right) \tag{6.5.4}$$

Note that in the code, the initialization of the choke opening is done in the output part, since the inputs (the pump flow in this case) aren't available in the initialization part.

6.6 Implementation of Choke Boundary

The choke provides the boundary condition for the system at x=l. The challenge is to solve for the boundary condition of the downward moving invariant $\beta(t,l)$. By adding 6.1.8 and 6.1.9, we get the topside boundary condition

$$\beta(t,l) \;=\; -\alpha(t,l) + 2(u-\bar{u}) \tag{6.6.1}$$

In early versions of the simulator, the assumption that the flow through the choke was always positive (upwards) was made. However, this resulted in permanent pressure drops in the system whenever the flow turned out to be otherwise, which happens when the back pressure pump is shut off, or the piston velocity is really high. We will consider the two cases separately here. First let's assume the flow is positive.

6.6.1 Positive Flow

When the flow through the choke is positive $p_c > p_0$ and we have from (5.3.2) and (5.3.2)

$$q_c = G(u_c)\sqrt{\frac{1}{\rho_L}(p_c - p_0)}$$

$$q_c = q_b + q_w$$

At the outlet $p_c = p(t, l)$ and $q_w = u(t, l)A$. Thus,

$$(q_b + u(t, l)A)^2 \frac{\rho_L}{G^2(u_c)} = p_c - p_0 \tag{6.6.2}$$

α is the Riemann-invariant corresponding to the upward-moving characteristic. Given $\alpha(t, l)$, we would like to solve for $\beta(t, l)$. By inserting (6.1.12) and (6.1.13) into (6.6.2), we get the nonlinear problem

$$ax^2 + b = \exp(-\frac{x}{c}) \tag{6.6.3}$$

Where

$$x = \frac{q_b}{A} + \bar{u} + \frac{\alpha + \beta}{2} \tag{6.6.4}$$

$$a = \frac{A^2 \rho_L}{G^2(u_c)(k + \bar{p})} \exp\left(-\frac{1}{c}\left(\frac{q_b}{A} + \bar{u} + \alpha\right)\right) \tag{6.6.5}$$

$$b = \frac{k + p_0}{k + \bar{p}} \exp\left(-\frac{1}{c}(\frac{q_b}{A} + \bar{u} + \alpha)\right) \tag{6.6.6}$$

x is the flow velocity at the boundary. Since we are assuming $q_c \geq 0$ we must seek a solution $x* \geq 0$.

6.6.2 Reverse Flow

When the water is flowing reversely through the choke, we must have $p_c < p_0$. The choke equation (5.3.2) becomes

$$q_c = -G(u_c)\sqrt{\frac{1}{\rho_L}(p_0 - p_c)}$$

By doing the same derivation as for the positive flow, we get the nonlinear problem

$$-ax^2 + b = \exp(-\frac{x}{c}) \tag{6.6.7}$$

In this case, we are looking for a negative x, since the flow direction is negative.

6.6.3 Solution Algorithm

Bisection is chosen as the numerical method to find the roots. It is implemented as follows

1. If $G(u_c) = 0$, let $x^* = 0$ and go to step 4.
2. If $b \leq 1$, there exists a solution for some $x^* \geq 0$, if not, we assume the flow is negative and go to step 3.

3. The search interval for the bisection is chosen to be $[0, \sqrt{(1-b)/a}]$ (since the right hand side of (6.6.3) is less than 1 in the right half plane).
4. The solution $x^* \geq 0$ is found by bisection of the equation (6.6.3).
5. $b > 1$, the flow is negative. There exists a solution of (6.6.7) for some $x^* < 0$.
6. The search interval for the bisection is chosen to be $[\sqrt{b/a}, 0]$ (since this is where the parabola intersects with the negative x-axis).
7. The solution $x^* < 0$ is found by bisection of the equation (6.6.7).
8. $\beta(t,l)$ and p_c are computed as follows

$$\beta(t,l) = -\alpha(t,l) + 2\left(x^* - \frac{q_b}{A} - \bar{u}\right) \tag{6.6.8}$$

$$p_c = \begin{cases} p_0 + \text{sgn}(x^*)\rho_L \left(\frac{Ax^*}{G(u_c)}\right)^2 & G(u_c) > 0 \\ (k+\bar{p})\exp\left(\frac{\alpha(t,l)+\frac{q_b}{A}+\bar{u}}{c}\right) & -kG(u_c) = 0 \end{cases} \tag{6.6.9}$$

Where sgn is the signum function.

6.7 Implementation of the Piston Boundary

Adding 6.1.8 and 6.1.9 as follows, yields the boundary condition for x=0.

$$\begin{aligned} \alpha(t,0) &= c\ln(\frac{k+p(t,0)}{k+\bar{p}}) + u(t,0) - \bar{u} \\ &= (\alpha(t,0) - \beta(t,0))/2 + u(t,0) - \bar{u} \\ &= -\beta(t,0) + 2(u_0(t) - \bar{u}) \end{aligned} \tag{6.7.1}$$

The default setting in the simulator is using the piston model described in 5.4. An experimental, dynamic model is also implemented, see the source code of the quasi-linear simulator for details.

6.8 Outputs

To enable outputs from arbitrary points along the copper pipe, linear interpolation functions were written for the simulator. The default setting is to match the outputs of the actual lab, but this can be changed by specifying the "Desired pressure outputs" vector in the parameter list.

The pump flow input is needed in the output part of the simulator, since the choke flow (FT3) is not a state of the system. Therefore, the "ssSetInputPortDirectFeedThrough" is set to 1 for these two inputs. The piston velocity is also used in the output to calculate the pipe inlet flow.

Chapter 7 Linearized Simulator

In order to explore the properties of linear observers on this system, and to see how the response of a linearized version of the system is in contrast to the quasi-linear version, a linearized version of the simulator was made. It is very much derived in the same way as the quasi-linear simulator, and is based on the same principle. The derivation follows.

Around $p = \bar{p}$ and $u = 0$, the system model becomes

$$\frac{\partial p}{\partial t} + \rho c^2 \frac{\partial u}{\partial x} = 0 \tag{7.0.1}$$

$$\frac{\partial u}{\partial t} + \frac{1}{\rho}\frac{\partial p}{\partial x} + f(u) + g\sin(\gamma) = 0 \tag{7.0.2}$$

In matrix notation $\mathbf{z_t} + \mathbf{A}(\mathbf{z})\mathbf{z_x} = \mathbf{0}$, when the friction and gravity is ignored for now (indices denoting partial derivatives)

$$\mathbf{z} = \begin{bmatrix} p & u \end{bmatrix}^{\mathbf{T}}$$

$$\mathbf{A}(\mathbf{z}) = \begin{bmatrix} 0 & \rho c^2 \\ \frac{1}{\rho} & 0 \end{bmatrix} \tag{7.0.3}$$

The eigenvalues and corresponding left eigenvectors of A are

$$\lambda^{(1,2)} = \pm c \tag{7.0.4}$$

$$\mathbf{l}^{(1,2)} = \begin{bmatrix} \frac{\pm 1}{\rho c} & 1 \end{bmatrix} \tag{7.0.5}$$

Proceeding like in (6.1.4) and (6.1.5), we get the two Riemann-invariants (7.0.6) and (7.0.7) along the two characteristic lines $\frac{dx}{dt} = \pm c$

$$\alpha(p,u) = \frac{1}{\rho c}(p - \bar{p}) + u - \bar{u} \tag{7.0.6}$$

$$\beta(p,u) = -\frac{1}{\rho c}(p - \bar{p}) + u - \bar{u} \tag{7.0.7}$$

Combining (7.0.6) and (7.0.7) results in the following relations

$$u = \frac{\alpha+\beta}{2} + \bar{u} \tag{7.0.8}$$

$$p = \frac{\rho c}{2}(\alpha-\beta) + \bar{p} \tag{7.0.9}$$

Differentiated with respect to x and t, and inserted into (7.0.1) and (7.0.2) yields:

$$\frac{\partial \alpha}{\partial t} = -c\alpha_x - f(u) - g\sin(\gamma) \tag{7.0.10}$$

$$\frac{\partial \beta}{\partial t} = c\beta_x - f(u) - g\sin(\gamma) \tag{7.0.11}$$

7.1 Piston Boundary

The piston boundary condition is handled in the same way as in 6.7.

7.2 Choke Boundary

The upper boundary, at the choke, is determined by the choke equation (5.3.2). We proceed like in 6.6, and consider the positive and negative flows separately. Just like in the quasi-linear case, we want to solve for the boundary value of the downward moving invariant. Once we know the fluid velocity, we can use

$$\beta(t,l) = -\alpha(t,l) + 2(u-\bar{u}) \tag{7.2.1}$$

x is defined in the same way as for the quasi-linear boundary value problem, so we still have

$$\beta(t,l) = -\alpha(t,l) + 2\left(x^* - \frac{q_b}{A} - \bar{u}\right) \tag{7.2.2}$$

7.2.1 Positive Flow

When the flow through the choke is positive $p_c > p_0$ and we have from (5.3.2) and (5.3.2)

$$q_c = G(u_c)\sqrt{\frac{1}{\rho_L}(p_c - p_0)}$$

$$q_c = q_b + q_w$$

At the outlet $p_c = p(t,l)$ and $q_w = u(t,l)A$. Thus,

$$(q_b + u(t,l)A)^2 \frac{\rho_L}{G^2(u_c)} = p_c - p_0 \tag{7.2.3}$$

α is the Riemann-invariant corresponding to the upward-moving characteristic. Given $\alpha(t,l)$, we would like to solve for $\beta(t,l)$. By inserting (7.0.6) and (7.0.7) into (6.6.2), we get the quadratic equation

$$K_1 x^2 + K_2 x + K_3 = 0 \tag{7.2.4}$$

Where

$$\begin{aligned} x &= \frac{q_b}{A} + \bar{u} + \frac{\alpha+\beta}{2} && (7.2.5)\\ K_1 &= -\frac{\rho A^2}{G^2(u_c)} && (7.2.6)\\ K_2 &= -\rho c && (7.2.7)\\ K_3 &= \bar{p} - p_0 + \rho c(\alpha(t,l) + u + \frac{q_b}{a}) && (7.2.8) \end{aligned}$$

Only the positive solution of the problem has a physical meaning in the case of positive flow.

7.2.2 Reverse Flow

It turns out that for reverse flow $p_c < p_0$, the only thing changing in the quadratic problem is the sign of K_1. In other words, the problem to be solved when the equation for positive flow doesn't result in a positive x is

$$K_1 x^2 + K_2 x + K_3 = 0 \tag{7.2.9}$$

Where

$$\begin{aligned} x &= \frac{q_b}{A} + u + \frac{\alpha+\beta}{2} && (7.2.10)\\ K_1 &= \frac{\rho A^2}{G^2(u_c)} && (7.2.11)\\ K_2 &= -\rho c && (7.2.12)\\ K_3 &= \bar{p} - p_0 + \rho c(\alpha(t,l) + u + \frac{q_b}{a}) && (7.2.13) \end{aligned}$$

And x has to be negative.

7.3 Comparison Between the Linear and the Quasi-Linear Simulator

The linear and the quasi-linear simulator were excited by the same input signals; a sine wave sweep over the frequencies 0Hz through 0.6Hz with a constant choke opening. The relative error was increasing with the frequency, and decreasing as the back pressure pump

flow was increased. The relative error of the bottom hole pressure estimate for the as 0.6Hz disturbance and no back pressure pump flow was about 1.5%. This suggests that the linearization is justifiable for our system, and should be used whenever run times are important.

7.4 Test of the Simulators

To get some numbers illustrating the benefits of writing the simulator in C-code, a test was done. The 3 different simulators (the m-version, the quasi-linear C-version, and the linear C-version) were excited with the same reference signal. They were ran for 20 seconds, and the time was recorded using MATLAB's tic/toc-function. The ode45 solver was used in all the simulations. The runtimes can be seen in table 7.4.1.

Complexity (N)	m-file	Quasi-linear C-MEX	Linear C-MEX
10 elements	361 s	0.15 s	0.1 s
100 elements	421 s	0.3 s	0.17 s
1000 elements	960 s	8 s	4.2 s

Table 7.4.1: *Results from the tests*

It is clear that the compiled C-code is advantageous for real-time performance compared to the interpreted MATLAB code.

Chapter 8 Parameter Identification

In this section, the necessary parameters for the model discussed in the previous chapters will be discussed, both theoretically and experimentally.

8.1 Numbers of Relevance

These are numbers that will be used in various derivations in this chapter.

Property	Value
BHA length	350 mm
BHA diameter	40.9 mm
Upper rod diameter	25 mm
Lower rod diameter	22 mm
Compartment length	1.7 m
Compartment diameter	42.53 mm

Table 8.1.1: *Dimensions of the piston with BHA1*

Property	Symbol	Value
Copper pipe coil radius	r_c	1.07 m
Copper pipe coil height	h_c	2.3 m
Copper pipe coil pitch	H	0.017 m
Copper pipe length	L	900 m
Copper pipe inner radius	r_p	8 mm
Water density	ρ	998 kg/m^3
Water viscosity	μ	$1.00 \cdot 10^{-3}$ $kg/(m \cdot s)$

Table 8.1.2: *Key numbers for friction*

8.2 Piston friction

Boge [6] did experiments to determine both theoretical and empirical pressure drop models for the piston part of the system. The resulting linear empirical equation for the pressure drop over the BHA was

$$\Delta P = -1.63 \cdot v(t) + 0.15 \; [bar]$$

Where v is the piston velocity in meters per second. To verify this result, and see if a linear model is sufficient, an experiment was conducted. The system was pressurized up to approximately 5 bar, and the choke was set to a 28 degree opening. Then a sine sweep was used as a reference signal for the piston. By differentiating the position reference, the pressure drop as a function of the fluid velocity was plotted, and is shown in figure 8.2.1.

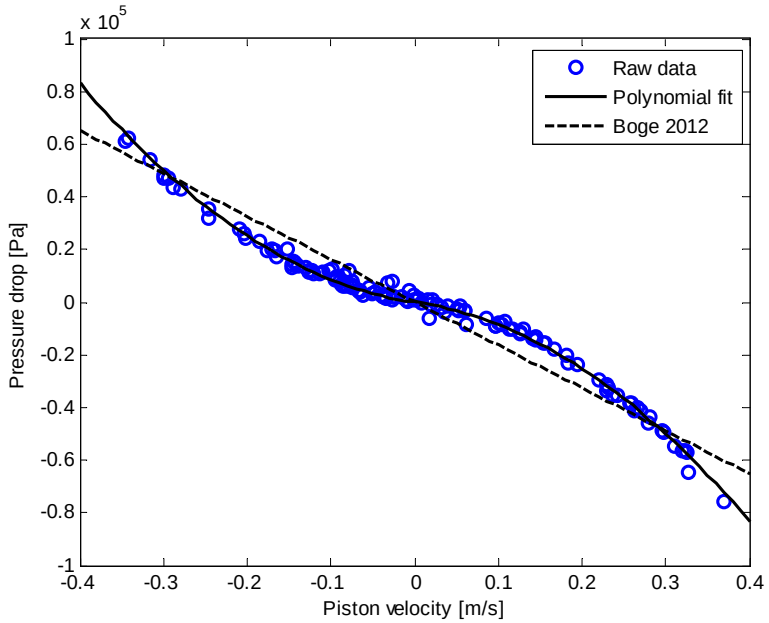

Figure 8.2.1: *The pressure drop over the BHA as a function of the piston velocity. Boge's linear pressure drop function is also shown.*

The curve was approximated by a function on the form

$$\Delta P = f_{d,1} \cdot v_d + f_{d,2} \cdot v_d \cdot |v_d| \tag{8.2.1}$$

where the constant parameters were found using the curve fitting tool in MATLAB.

The coefficients

$$\begin{aligned} f_{d,1} &= -43840 \; [Pa \cdot s/m] \\ f_{d,2} &= -410400 \; [Pa \cdot (s/m)^2] \end{aligned}$$

gave a good fit. There seems to be no significant time delays between the piston velocity and the pressure drop.

Note: the dynamics have been ignored in this parameter identification for severeal reasons. Firstly, due to problems with one of the flow meters needed for this (FT4), secondly, fewer parameters make it easier to get results close to the ones in the lab.

The alternative piston model 5.4.1 was also tuned to fit the lab, resulting in the linear piston friction 3000, and the quadratic friction 9000.

8.2.1 Verification

The polynomial from the previous paragraph tested on data from a sine sweep with a 70 degree choke opening is shown in figure 8.2.2.

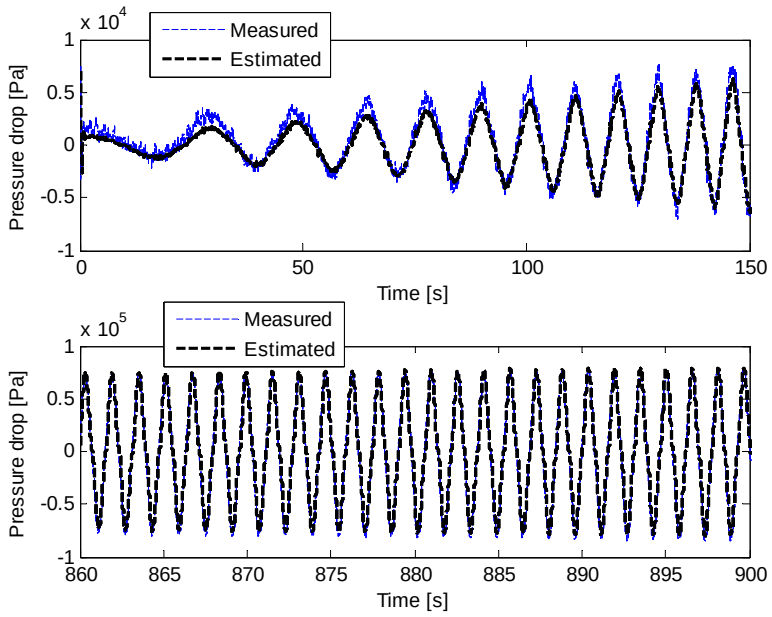

Figure 8.2.2: *The empirical pressure drop function compared to measurements from the rig*

8.3 Propagation Speed in the Copper Pipe

The speed of sound is the number determining how fast pressure waves propagate in the pipe.The theoretical speed of sound in water in an infinite fluid medium is about 1484 m/s, but this isn't necessarily true for pipe flow.

8.3.1 Theory

Pipe walls are known to slow down pressure waves, and especially when the fluid being carried is a liquid. A correction formula [30] is:

$$c_{pipe} = \frac{c}{\sqrt{1 + \kappa \frac{\beta}{E} \frac{2d}{d_0 - d}}} \tag{8.3.1}$$

where c is the speed of sound in an infinite fluid medium (m/s), β is the bulk modulus of the fluid (Pa), E is the Young's modulus of elasticity of the wall material (Pa), d is the internal diameter of the pipe (m), d_0 is the external diameter of the pipe (m), and κ is a coefficient in the range $0 \leq \kappa \leq 1$, which is zero when wall effects are negligible, but is unity when the pipeline contains expansion joints. This formula predicts a speed of sound at 1353 m/s for the case with $\kappa = 1$ and $E = 117$ GPa.

8.3.2 Experiment

Different approaches to determining the wave speed in the system were considered. Among them, measuring the compressibility by pressurizing the system, and measuring the volume change, and measuring the transient propagation speed in the system. The last one was chosen, since this was considered the easiest, and the most accurate.

Data from 12 earlier experiments were used. The time lag between the transients of the pressure disturbance at x=0 and x=900m were measured by hand (from PT10 to PT1). This yielded the numbers in table 8.3.1.

Propagation time from P1 to C2	Speed of sound
0.70 s	1286 m/s
0.91 s	989 m/s
0.76 s	1184 m/s
0.83 s	1084 m/s
0.74 s	1216 m/s
0.74 s	1216 m/s
0.76 s	1184 m/s
0.75 s	1200 m/s
0.75 s	1200 m/s
0.77 s	1169 m/s
0.78 s	1154 m/s
0.75 s	1200 m/s

Table 8.3.1: *Speed of sound measurements*

Which results in an mean value of $c = 1173$ $[m/s]$ with a standard deviation of 74.5. This value is certainly lower than the theoretical value (1353 m/s). This may be caused by entrained air in the water [31]. If there is a mix of water and air in the system, where the volume of each component is denoted by V_{air} and V_{water} respectively, such that

$$\Delta V = \Delta V_{air} + \Delta V_{water} \tag{8.3.2}$$

and

$$\rho = \rho_{air}\frac{V_{air}}{V} + \rho_{water}\frac{V_{water}}{V} \tag{8.3.3}$$

the bulk modulus of the mixture, defined as

$$\beta = \frac{\Delta p}{\Delta V/V} \tag{8.3.4}$$

becomes

$$\beta = \frac{\beta_{water}}{1 + (V_{air}/V)(\beta_{water}/\beta_{air} - 1)} \tag{8.3.5}$$

Using the definition of the speed of sound

$$c = \sqrt{\frac{\beta}{\rho}} \tag{8.3.6}$$

we can show the relation in a plot:

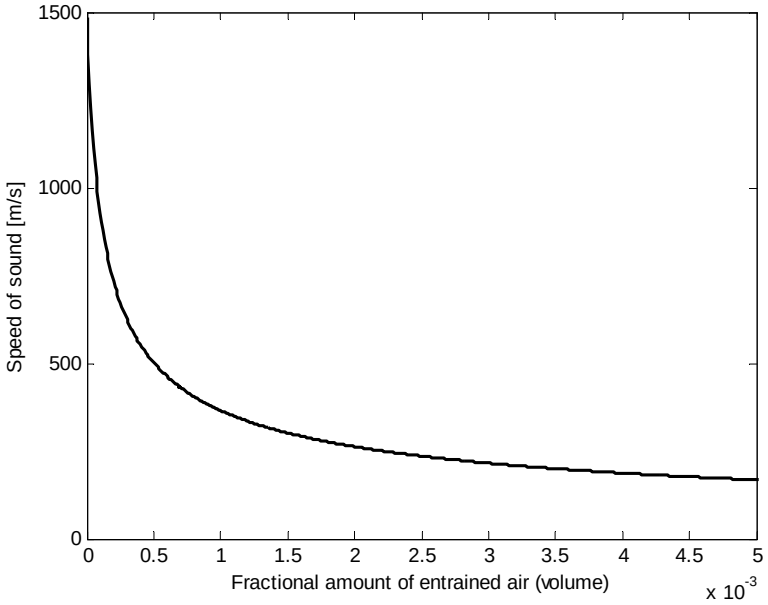

Figure 8.3.1: *Speed of sound as a function of fractional amount of entrained air*

This indicates that even a small amount of air may cause the speed of sound to differ significantly from the tabular value. Another option is that the rubber sections of the tubing may cause a decrease of the wave speed due to their elasticity, but this was considered unlikely to cause the discrepancy, since the propagation time within the copper pipe (from PT1 to PT10) is exactly the same as the propagation time with the additional rubber pipes (from P1 to C2).

To consider the theoretical effect of elasticity in the pipes, we have to make an assumption. Young's modulus is not really applicable to nonlinear materials, such as rubber, unless the strains are small. We will assume linearity so we can calculate a ball-park estimate on the effect they have on the overall wave propagation speed in the system.

The system has about 6.6 meters of rubber pipe (2.6 meters before the copper pipe inlet, and several portions, totally 4 meters after the copper pipe outlet), and about 2.5 meters of PVC pipes between the copper pipe outlet and the choke. The Young's modulus for rubber is somewhere around 0.01-0.1 GPa (we will use the mean value) and for PVC it is about 1.5 GPa. The inner and outer diameter of the rubber and PVC pipes are (19x29mm) and (19x25mm) respectively, yielding the velocities

$$\begin{aligned} c_{rubber} &= 120\ [m/s] \\ c_{PVC} &= 462\ [m/s] \end{aligned}$$

Since the portions of the pipe are only a few meters long, this velocity change is not very noticeable by measuring the propagation speed of a wave (the additional time delay the elastic tubes imply, is about 0.02-0.025s).

The bulk modulus of the system (including the rubber tubes) was determined experimentally by Boge [7], resulting in a value around 1.5E9 Pa^{-1},which implies a propagation speed of 1225 m/s, which is within one standard deviation from the value found by measuring propagation speed. However, it was also found indications that the bulk modulus was a function of the pressure in the system, this may be caused by the nonlinear nature of the rubber pipes.

8.4 Choke Characteristic

To determine the choke characteristic $G(u)$, a series of steps in the choke opening reference was applied, and $G(u)$ was plotted against u in MATLAB

$$G(u) = q_c / \sqrt{\frac{1}{\rho_L}(p_c - p_0)} = FT3 / \sqrt{\frac{1}{\rho_L}(C2 - C1)}$$

resulting in the functions seen in figure 8.4.2. As can be seen, there is almost no difference between the opening and the closing characteristic. This clearly shows that the deadband discovered last fall is practically eliminated.

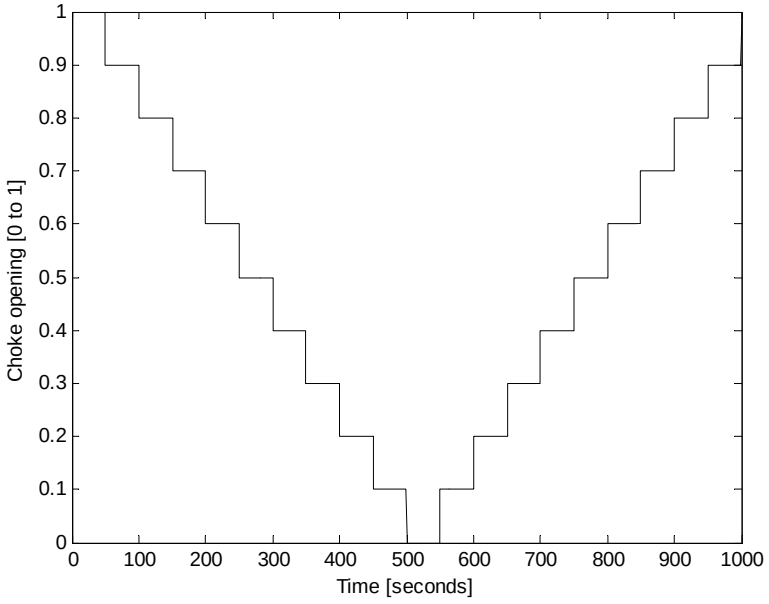

Figure 8.4.1: *Choke reference signal*

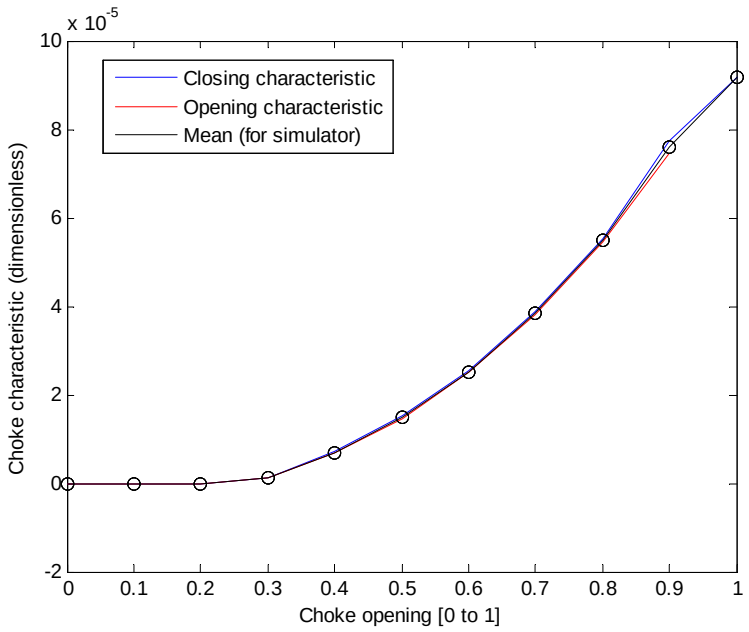

Figure 8.4.2: *Choke characteristics for opening and closing*

The mean of the two characteristics was calculated, and the values were interpolated by a cubic spline on an even grid, resulting in a vector to be used in the simulator.

The time delay associated with opening and closing the choke (from 0 to 90 degrees and vice versa) was measured to about 1 second, as shown in figure 8.4.3.

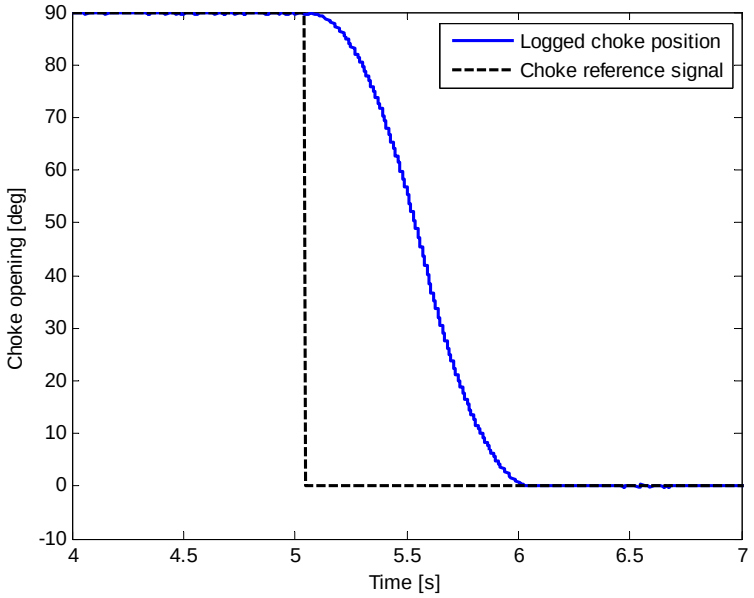

Figure 8.4.3: *Choke time response*

Some selected value from the resulting characteristic are shown in table 8.4.1.

0	15	20	25	28	31	40	50	60	70	80	90
0	0	2.2E-7	8E-7	2.5E-6	4.5E-6	1.19E-5	2.3E-5	3.69E-5	5.76E-5	8.66E-5	1.03E-4

Table 8.4.1: *A selection of values from the choke characteristic. The entire characteristic is found in the parameter list in the simulator.*

8.4.1 The Use of the Choke Characteristic for Unsteady Flows

The choke equation (5.3.2) (also known as the orifice equation) can be derived from Bernoulli's equation. However, Bernoulli's equation strictly requires the flow to be steady, which is not the case for our simulations.

In figure 8.4.4, the flow through the choke is calculated for two different experiments, with the same choke opening and disturbance frequency, but with the pump enabled only in the upper one.

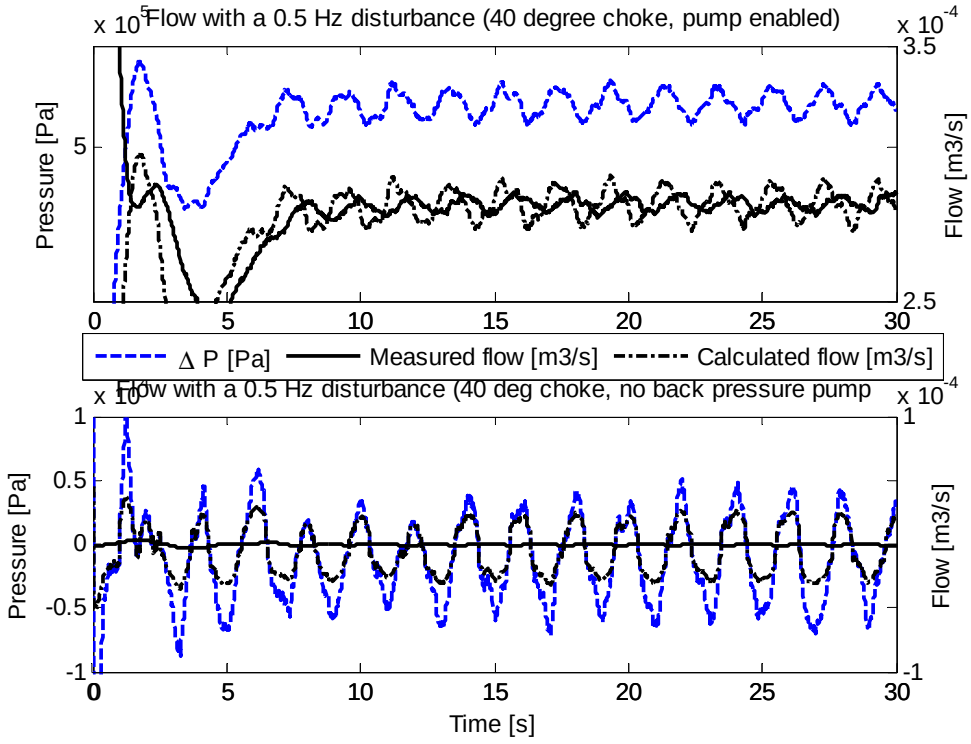

Figure 8.4.4: *Choke characteristics verification. Both the experiments were with a 40 degree choke opening and a 0.5 Hz disturbance.*

As can be seen, the steady flow-part of the flow is accurately calculated using the choke characteristic. When the back pressure pump is disabled, there is no steady-state differential pressure, which makes the flow calculations very inaccurate. This suggests that the simulator is best suited for experiments with the pump enabled. The main reason behind the discrepancy in the lower plot might be the lower flow limit for the flow meter. In any case, the actual flow seems to be phase-shifted from the pressure difference. This behavior

is not captured using the choke characteristic. This experiment, however, was done with a higher disturbance frequency than the lab is intended for.

8.5 Back Pressure Pump Flow

The pump flow measurements from the choke characteristics identification were used to identify the flow supplied by the back pressure pump, and see how it varies with the choke pressure. The graph in 8.5.1 is for the pump at 100%.

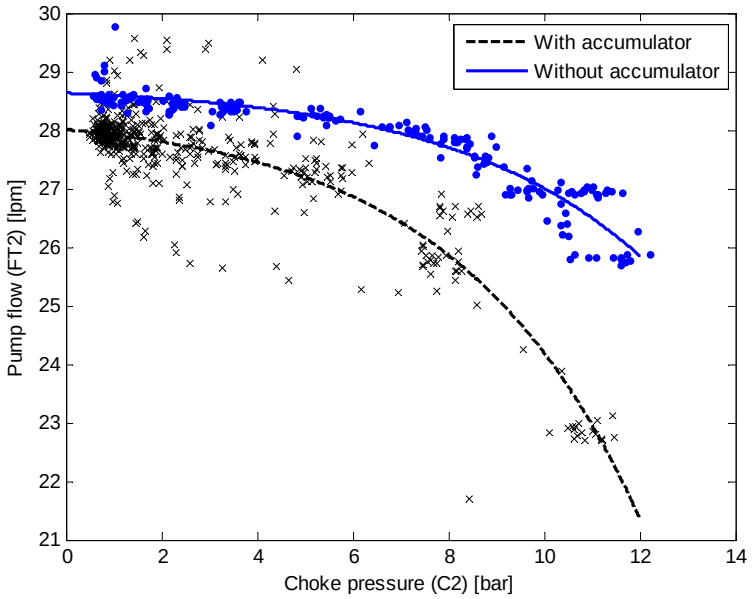

Figure 8.5.1: *The pump flow (FT2) vs the choke pressure (C2)*

As can be seen, the pump flow is falling as the pressure increases. This effect, however, was reduced greatly by removing the pump accumulator. If this effect turns out to be important to get accurate simulations, there is a simulink subsystem prepared for this purpose. The flow with the accumulator removed was fitted by the function

$$q_b = a \exp(-bp_c) + c; \tag{8.5.1}$$

With

$$\begin{aligned} a &= -2.4050e-06 \\ b &= -2.5070e-06 \\ c &= 4.7967e-04 \end{aligned}$$

The flow for different pump settings with an open choke was measured

Pump power [%]	0	10	20	30	40	50	60	70	80	90	100
FT2 flow [lpm]	11.7	11.7	11.7	11.8	11.9	12	17.3	20	22.7	25.8	28.4

Table 8.5.1: *Pump flow with open choke*

For low pump settings, the only flow is that supplied by the feeding pump (when the choke is open). The back-pressure pump flow starts at about 40% power.

8.6 Pipe friction

In this section, some theory will be presented first, and an estimated friction factor will be calculated, using a steady flow approximation. The approximation will then be tested on lab data.

8.6.1 Reynolds Number

The Reynolds number is given by

$$Re = \frac{\rho u d}{\mu} \tag{8.6.1}$$

First, we have to find out what the highest fluid velocity in the copper pipe is. The maximum speed of the piston, with a sinusoidal reference signal, is given by $v_{max} = 2\pi Af$ where A is the amplitude and f is the frequency in Hz. The fastest reference frequency during this project was 0.650 Hz, with a 0.1 m amplitude, resulting in a maximum piston velocity at 0.41 m/s, and a maximum fluid velocity 0.2249 m/s. This will generate a volumetric flow of about $q_{p\,max} = v_{max}(A_d - A_{d2})$ (see 5.4.1), in this case $q_{p\,max} = 4.5 \cdot 10^{-5}$ $[m^3/s]$ which results in the maximum fluid velocity in the pipe $u_{max} = q_{p\,max}/A_{pipe}$, here, since the inner pipe diameter is 16 mm, $u_{max} = 0.22$ $[m/s]$. Thus, the maximum Reynolds number in the copper pipe is about 3600, meaning the flow in the copper pipe is laminar for low frequency disturbances, and in the transition for the highest frequencies (2300<Re<4000).

This, however, is true around the piston. Compressibility effects in the copper pipe seem to slow down the flow. We will therefore only consider the laminar case in the rest of this section.

8.6.2 Friction Considerations

Results from literature show that when the flow is laminar (Re<2300), the friction factor is independent of the roughness of the pipe. The shear stress at the walls of the pipe is

$$\tau = \frac{f\rho u^2}{2} \tag{8.6.2}$$

and f (Fanning friction factor) for laminar flow in round tubes is taken to be

$$f = \frac{16}{Re} \tag{8.6.3}$$

However, the copper pipe is helical, and the friction factor in helical coils is also dependent upon the curvature ratio, λ and the Dean number [23], Dn given by

$$\lambda = \frac{\frac{r_c}{r_p}}{(\frac{r_c}{r_p})^2 + (\frac{H}{2\pi r_p})^2} \tag{8.6.4}$$

$$Dn = Re\sqrt{\lambda} \tag{8.6.5}$$

Where H is the pitch of the helix.

A widely used correlation due to Hasson (1955) for pipes of small curvature and negligible torsion is

$$f = \frac{16}{Re}(0.556 + 0.0969\sqrt{Dn}) \tag{8.6.6}$$

for $22 < Dn < 2000$

This makes our friction factor a nonlinear function of velocity. In terms of the pressure drop due to friction, we multiply the shear stress by wall area of the pipe, and divide by the cross-sectional area

$$f(u) = \frac{1}{\rho}\frac{2\pi r}{\pi r^2}\tau$$

then we insert 8.6.6 and the definition of the Reynolds number, and simplify.

$$\begin{aligned} &= \frac{1}{\rho}\frac{2\pi r}{\pi r^2}\frac{\rho u^2}{2}\frac{16\mu}{\rho u d}(0.556 + 0.0969\sqrt{Dn}) \\ &= \frac{8\mu u}{\rho r^2}(0.556 + 0.0969\sqrt{Dn}) \\ &= 0.0695u + 0.4512u^{3/2} \end{aligned} \tag{8.6.7}$$

Which is a nonlinear function of the fluid velocity. The flow speeds in the copper pipe are always less than about 0.2 m/s. In this area, the calculated friction can be approximated by the quadratic function

$$f(u) = 0.15u + 0.63u|u| \tag{8.6.8}$$

Or by the linear function

$$f(u) = 0.2446u \tag{8.6.9}$$

The three functions are shown in figure

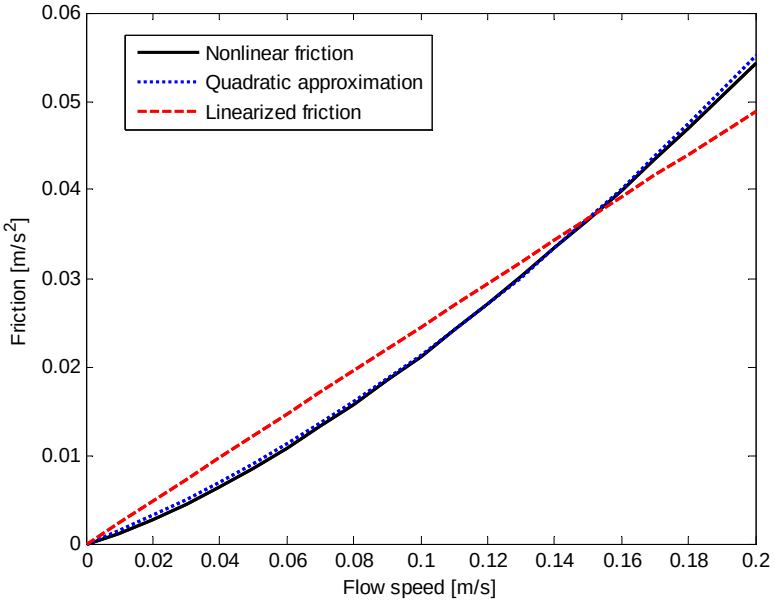

Figure 8.6.1: *Friction functions*

8.6.3 Friction from Experiments

An experiment was conducted to determine the actual steady-state friction in the lab. The choke was shut off to pressurize the system, and the valve in the bottom of the piston compartment was opened slightly (about 10 degrees). Then, the flow rate was adjusted by changing the pump power. This was done a few times to get a rich data set. The pressure drops for each sensor was calculated by subtracting the hydrostatics and sensor bias from previous experiments with the system filled with water

Then the steady-state portions of the resulting data were averaged. Equation (5.2.3) for a constant flow yields

$$\frac{c^2}{k+p}\frac{\partial p}{\partial x} + f(u) = 0 \tag{8.6.10}$$

By using $\frac{\partial p}{\partial x} = \frac{P(900)-P(0)}{900}$ and $p = \frac{P(900)+P(0)}{2}$, an approximate of the friction term was calculated. The best line fit in the least squares sense, intersecting the origin was

$$f_1 u = 0.2412u \tag{8.6.11}$$

(compare to (8.6.7))

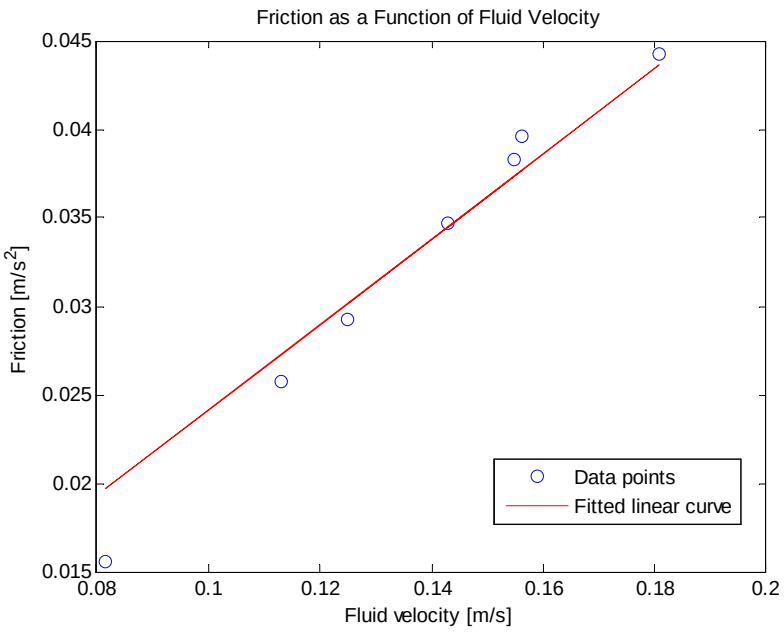

Figure 8.6.2: *Pipe friction plotted against the fluid velocity in the pipe*

This frequency function fits the data in the steady portions of the data set shown in figure 8.6.3.

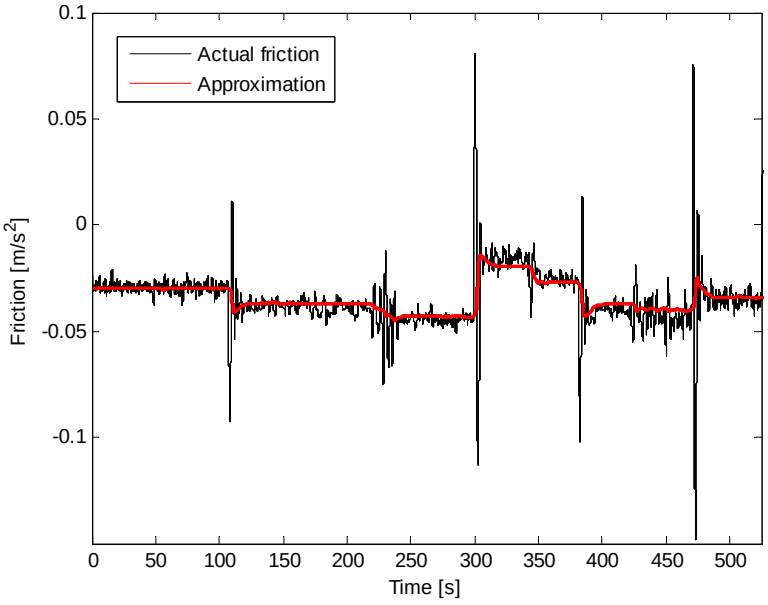

Figure 8.6.3: *Verification of the friction result . Here all the terms of (5.2.3), except the friction are calculated by approximating the derivatives, and are plotted against -$f_1 u$. The flow was assumed homogeneous throughout the pipe in the calculations. The black graph is an ensemble average based on data from all the pressure sensors.*

However, this friction term is based on the assumption of constant flow. We will look into what effects unsteady flow may have on the flow in the next section.

8.6.4 Transient Effects

During acceleration and deceleration of the water, there are likely to be transient friction effects not modeled so far.

Several papers describe algorithms to determine the unsteady friction. They are either dependent upon [5]

- The instantaneous mean flow velocity u
- The instantaneous mean flow velocity u and the instantaneous local acceleration $\partial u/dt$
- The instantaneous mean flow velocity u, the instantaneous local acceleration $\partial u/dt$ and the instantaneous convective acceleration $\partial u/dx$
- The instantaneous mean flow velocity u and diffusion$\partial^2 u/dx^2$
- A cross-sectional distribution of instantaneous flow velocity.
- The instantaneous mean flow velocity u, and a weighted sum for the past velocity changes

[10] investigates the relative importance of unsteady friction on the damping as a function of the dimensions of the system. The article shows that the importance of unsteady damping is decreasing when the length/diameter ratio increases. This might indicate that unsteady friction is not that important in our setup, due to the large ratio. However, since the results are not based on pure oscillatory flow conditions, they are not directly applicable to the lab.

A frequency model worth considering for the simulator if an unsteady friction function is going to be implemented in the future, is the Brunone et al (1991) model

$$f_u = k(\frac{\partial u}{\partial t} + \text{sgn}(u)c\left|\frac{\partial u}{\partial x}\right|) \tag{8.6.12}$$

which can be implemented with the method of characteristics, the interested reader may read [22] for a derivation. It is interesting to notice that the unsteady friction contributes to the phase of the pipe system.

Chapter 9 Tuning

This section is dedicated to tuning the simulator to get the frequency response as similar to the lab's as possible.

9.1 Tuning Choices

In a series of experiments conducted in collaboration with Martin Standahl Gleditsch, the lab rig was excited by sine sweeps, one for each choke opening, resulting in the surface seen in figure 9.1.1. In addition, an experiment was done where the pipe was terminated at the end of the copper pipe (avoiding rubber tubes). Data from this experiment is included in figure 9.1.2. Our goal will be to get the frequency response of the bottom hole pressure as similar to the lab's as possible, since this is considered the most important state of the system. The frequency responses shown are depicting the ratio BHP/piston position.

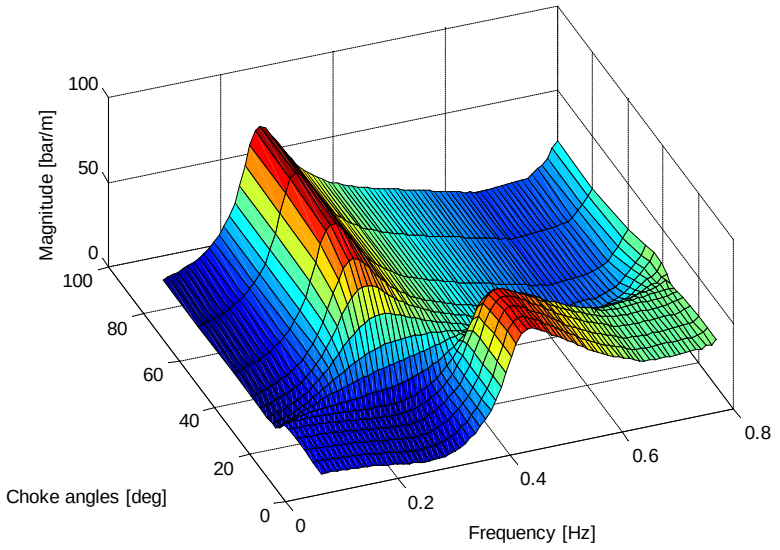

Figure 9.1.1: *Frequency response of the lab rig (courtesy of Martin Standahl Gleditsch)*

The reason why the piston position was chosen, and not the piston velocity, as one would expect, is first of all, that in the lab, only the position data is available for the piston, so it is

easier to just use the measurement instead of differentiating the noisy signal. But secondly, the transfer function from velocity to bottom hole pressure amplitude starts off with an infintely high magnitude. This can be understood by considering what happens when the piston is moved with a constant velocity (zero frequency). This will pressurize the system infintely. When the transfer function from position is used, we get a step instead of an impulse.

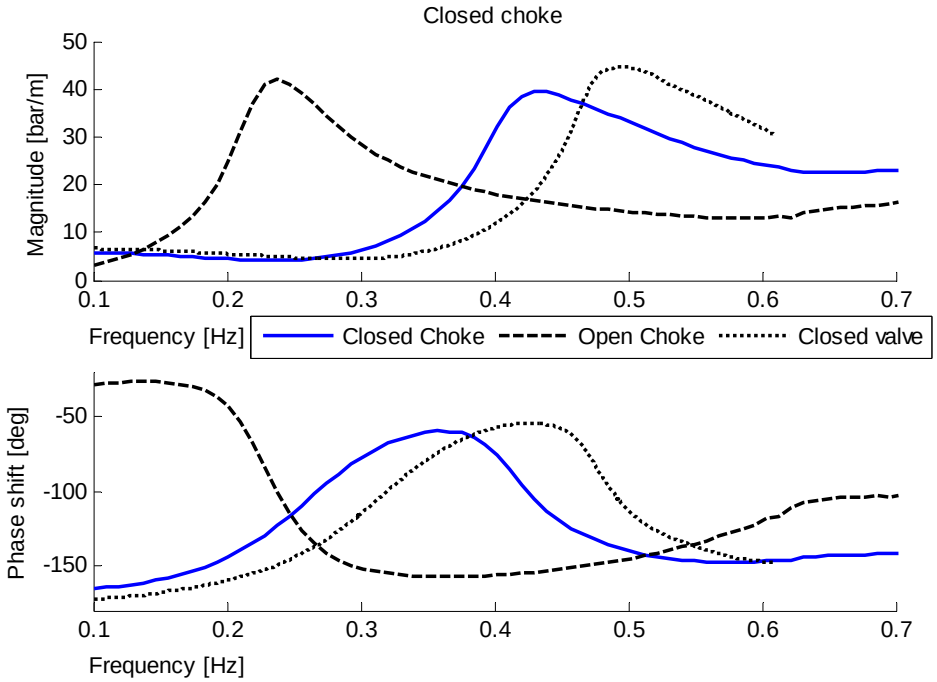

Figure 9.1.2: *Frequency response for open and closed chokes, and with different terminators in the closed case.*

The choke-terminated experiment resulted in resonance peaks at about 0.44 Hz and 0.25 Hz, for closed and open choke respectively. When the line is terminated by the valve after the copper pipe, the resonance moves up to about 0.49 Hz.

These resonance peaks correspond to a lower wave speed than the one identified. This will be looked more into in the next subsections.

9.2 Frequency Response of the System

To ease analysis of the system, an analytic expression for the frequency response of the system was derived, with the linear dynamics in 7.0.1 and 7.0.2 as basis.

In addition, a friction term ($f_2 u_t$) dependent upon the temporal fluid acceleration was added to see how this affects the frequency response (a more realistic model would be dependent upon the sign of the flow). The gravity bias was removed by defining

$$\bar{p}(x,t) = p(x,t) + \rho g \sin(\gamma) x \tag{9.2.1}$$

Then the model was restated as

$$\frac{\partial \bar{p}(x,t)}{\partial x} = -\rho \frac{\partial u(x,t)}{\partial t} - f_1 u(x,t) \tag{9.2.2}$$

$$\frac{\partial u(x,t)}{\partial x} = -\frac{1}{\rho c^2} \frac{\partial \bar{p}(x,t)}{\partial t} \tag{9.2.3}$$

with the linearized boundary conditions

$$p(l,t) + ku(l,t) = 0 \tag{9.2.4}$$

$$u(0,t) = -v_d(t) \frac{A_d - A_{d2}}{A} = -v_d(t) A_2 \tag{9.2.5}$$

By interchanging integration and derivation, we can obtain the Laplace transformed system equations

$$\frac{\partial \bar{P}(x,s)}{\partial x} = -\rho(f_1 + s) U(x,s) \tag{9.2.6}$$

$$\frac{\partial U(x,s)}{\partial x} = -\frac{s}{\rho c^2} \bar{P}(x,s) \tag{9.2.7}$$

This is a system on the form

$$\frac{\partial Z(x,s)}{\partial x} = A(s) Z(x,s) \tag{9.2.8}$$

which has the general solution

$$Z(x,s) = \exp(A(s)x) \Lambda(s) \tag{9.2.9}$$

Using MATLAB's symbolic toolbox, and rewriting in terms of hyperbolic functions, the matrix exponential can be found

$$\exp(A(s)x) = \begin{bmatrix} \cosh(\kappa x) & -\frac{c^2 \kappa \rho \sinh(\kappa x)}{s} \\ -\frac{s \sinh(\kappa x)}{c^2 \kappa \rho} & \cosh(\kappa x) \end{bmatrix} \tag{9.2.10}$$

Where

$$\kappa = \frac{\sqrt{s(f_1 + s)}}{c} \tag{9.2.11}$$

By applying the boundary conditions, we can solve for Λ.

$$\Lambda(s) = -A_d V_d(s) \begin{bmatrix} \frac{\rho c^2 \kappa \sinh(\kappa l) + k \cosh(\kappa l) s}{\rho c^2 \cosh(\kappa l) s + k \sinh(\kappa l) s^2} \\ 1 \end{bmatrix} \tag{9.2.12}$$

And finally, the transfer function from $V_d(s)$ to the bottom hole pressure$P(0,s)$

$$\frac{P(0,s)}{V_d(s)} = -\frac{\mathrm{A}_2\kappa\rho c^2\left(\kappa\rho \mathrm{c}^2\sinh\left(\kappa l\right) + k\cosh\left(\kappa l\right)s\right)}{\kappa\rho c^2\cosh\left(\kappa l\right)s + k\sinh\left(\kappa l\right)s^2} \tag{9.2.13}$$

This is an irrational transfer function, and to be of any use in simulations, it needs to be approximated by a rational model. This may be done by e.g writing the irrational terms as infinite series, and truncate. This transfer function is derived in terms of impedances in [11].

9.3 Parametric analysis

9.3.1 Variation of the Speed of Sound

The speed of sound is related to the frequencies of the resonance peaks. We may calculate the poles of the transfer function 9.2.13 in the two cases k=0 (choke closed) and k=inf (choke open). If we neglect friction for a second, the resonances for the open choke case occur when

$$\cosh(\kappa l) = 0 \tag{9.3.1}$$

which is true whenever

$$f = n\frac{1}{4}\frac{c}{l},\ n = 0, 1, 2\ldots \tag{9.3.2}$$

And when the choke is closed, whenever

$$\sinh(\kappa l) = 0 \tag{9.3.3}$$

which happens when

$$f = n\frac{1}{2}\frac{c}{l},\ n = 0, 1, 2\ldots \tag{9.3.4}$$

The resonance peaks of the lab happens when $f = 0.24$ when the choke is open, and at $f = 0.43$ when the choke is closed. This indicates a speed of sound at 782 m/s in the closed choke case and 873 m/s in the open choke case. In figure 9.3.1, it is shown how adjustment of the speed of sound affects the frequency response of the system.

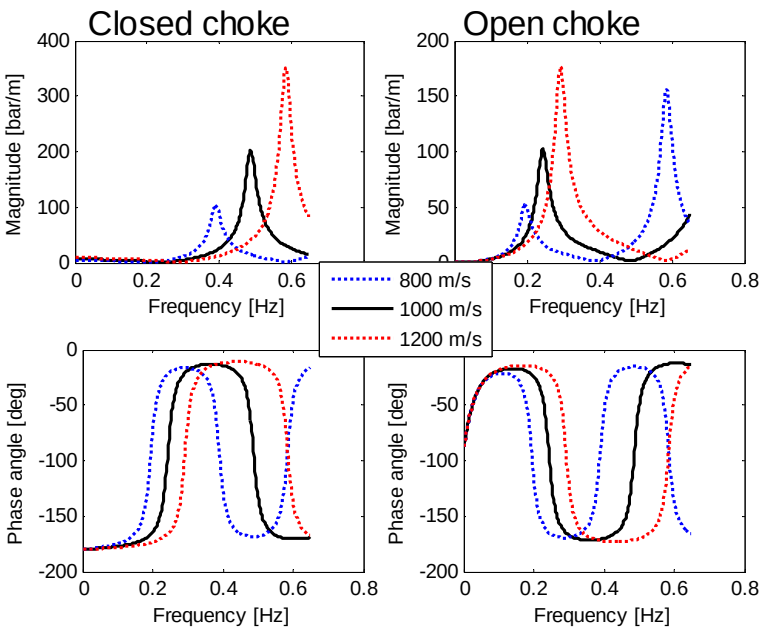

Figure 9.3.1: *Adjustment of the speed of sound.*

9.3.2 Variation of the Pipe Friction

The linear pipe friction's contribution is damping, that is, lowering the resonance peaks. As can be seen in the figure below, the friction as a function of the flow velocity does not move the resonance peaks at all.

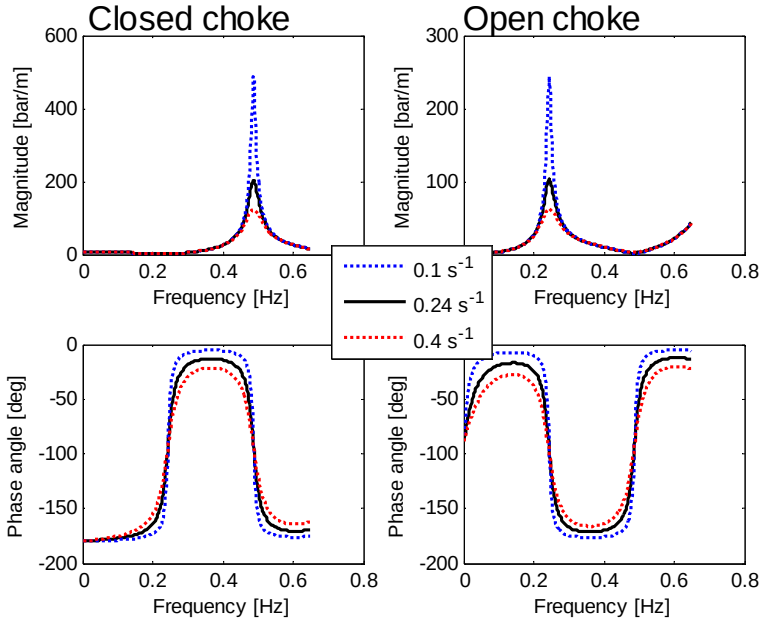

Figure 9.3.2: *The resonance peaks are higher for lower linear pipe friction*

9.3.3 Variation of the Choke Leakage

Using the quasi-steady simulator, the flow coefficient for the smallest choke opening was adjusted to see how this affects the frequency response. Note that this simulation was not done with the same parameters as the previous plots. The frequency response looks slightly different from the theoretical one since it is generated by applying a sine sweep which does not necessarily produce the exact frequency response.

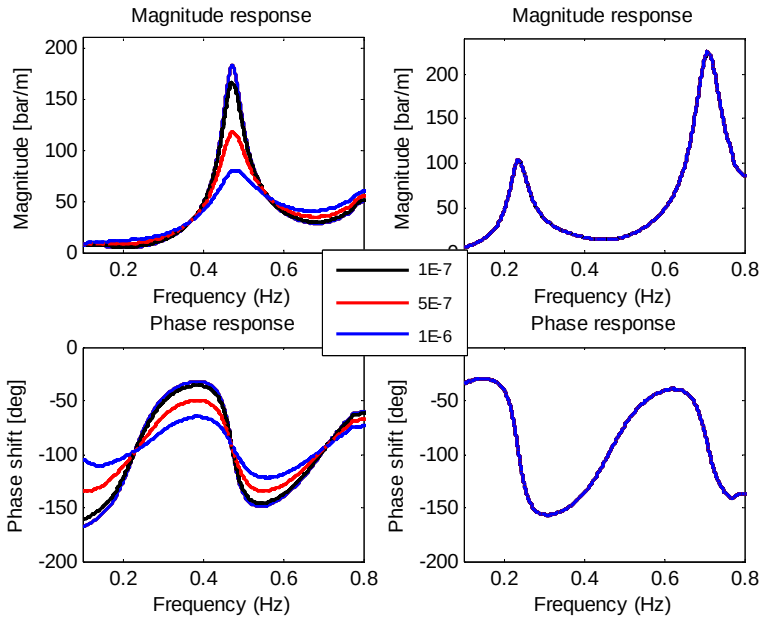

Figure 9.3.3: *Increasing the minimum flow coefficient ("leak"-flow) lowers the resonance peaks for the closed choke case. Closed choke to the left, open choke to the right.*

The resonance peaks for the closed choke case are not surprisingly lowered. The phase response is also flattened as the leakage gets bigger.

9.4 Fine tuning

The goal of the tuning was to get the frequency response from the piston disturbance to the bottom hole pressure as similar as possible. First of all, to get a lower resonance peak when the choke is closed, a small offset was added to the choke characteristic for the zero values. This can be justified by observing a slow gradual pressure drop when the system is pressurized and the choke is closed. Secondly, to get the resonance peaks moved towards lower frequencies, the speed of sound was lowered.

A comparison of the actual frequency response, and that of the simulator is shown in figure 9.4.1.

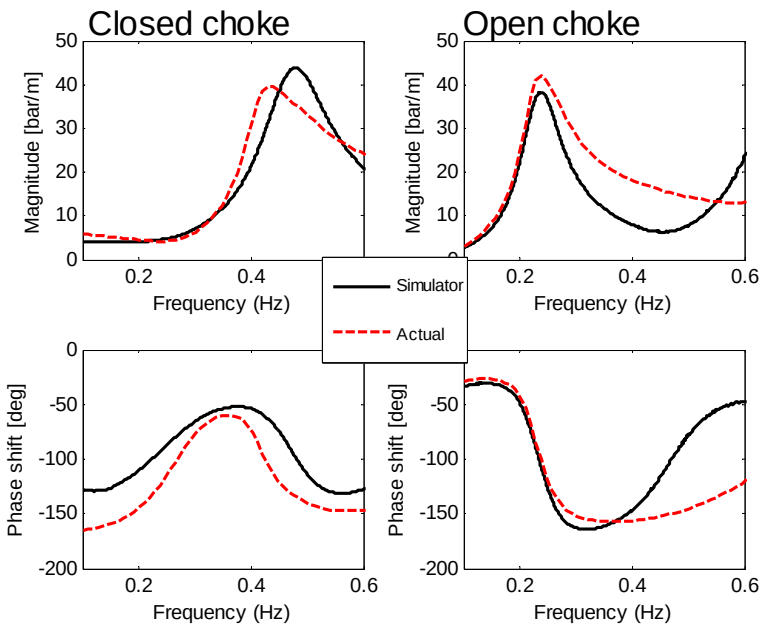

Figure 9.4.1: *Comparison of the simulator frequency resonse and the real response. Closed choke to the left, open choke to the right.*

As can be seen, the simulator gives a pretty good estimate for the behavior of the system for low frequencies. The modeling errors get worse for higher frequencies in both cases.

9.4.1 Parameter values

These are the final simulator parameters after tuning to get the best fitting frequency response in experiments without the back pressure pump.

Parameter name	Identified value	Calculated value	After tuning
Speed of sound	1173 [m/s]	1353 [m/s]	850 [m/s]
Piston linear friction	-43840 $[Pa \cdot s/m]$	-	-43840 $[Pa \cdot s/m]$
Piston quadratic friction	-410400 $[Pa \cdot (s/m)^2]$	-	-410400 $[Pa \cdot (s/m)^2]$
Linear pipe friction	0.2412 $[1/s]$	0.15 $[1/s]$	0.15$[1/s]$
Quadratic pipe friction	-	0.63	0.63
Leak adjustment	Not measureable	-	6E-7

Table 9.4.1: *Identified parameters and parameters after tuning*

9.5 Time responses

The simulator was excited with the same data as the lab, and comparative plots of the time response follow.

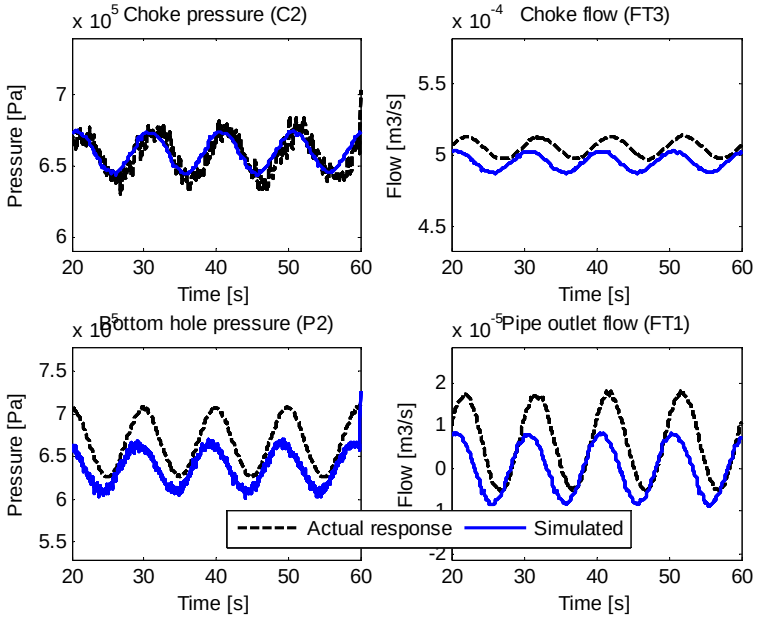

Figure 9.5.1: *Simulator response. The disturbance frequency is 0.1 Hz and the choke opening is 50 degrees.*

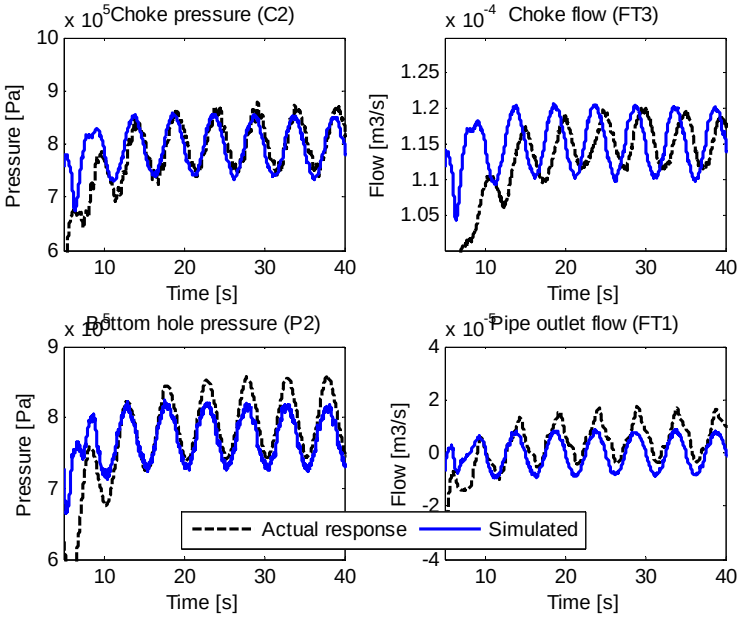

Figure 9.5.2: *Simulator response. The disturbance frequency is 0.2 Hz and the choke opening is 31 degrees.*

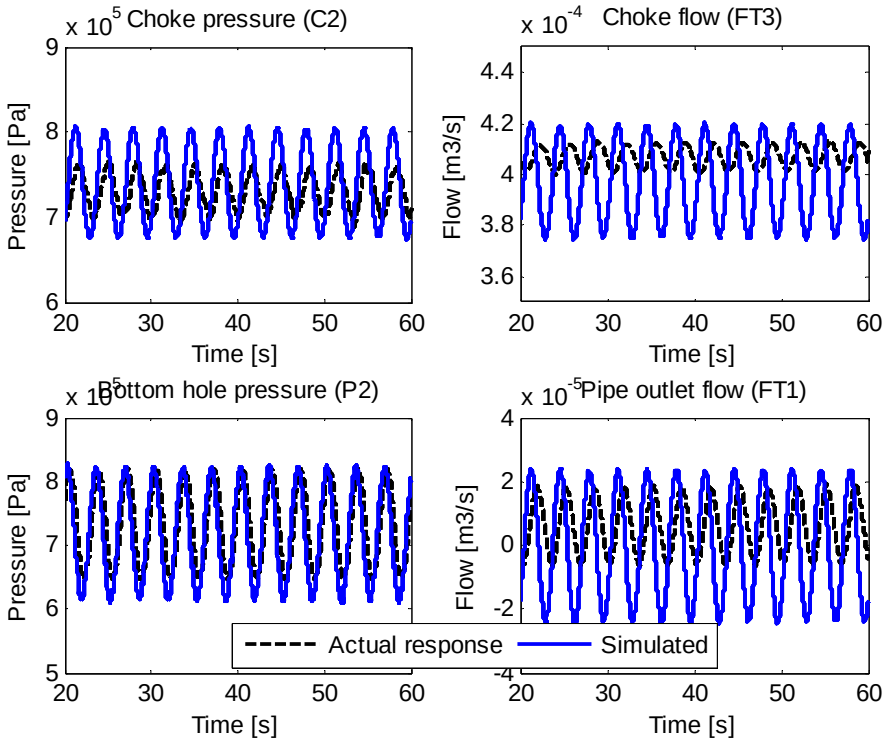

Figure 9.5.3: *Simulator response. The disturbance frequency is 0.3 Hz and the choke opening is 45 degrees.*

From these time responses, a few things are clear. Firstly: there is a phase error, which seems to be largest in the simulated choke flow (FT3). This is likely to be caused by the steady-flow simplification used (see 8.4.1). There is also an error in the amplitudes of the time responses, which again seems to be most significant for the choke flow. Notably, the bottom hole pressure is consistently the least erroneous signal. This is of course because the simulator was tuned to get this estimate right.

Chapter 10 Observer Implementation

10.1 Backstepping Observer

The ultimate goal for the observer design is to be able to determine the bottom hole conditions solely based on topside measurements. The first observer implemented is [4]. This is already derived for the system 7.0.1, but has not been tested in the lab or with a quasi-linear model. A short summary of the observer design follows.

Consider an observer on the form

$$\begin{aligned}
\hat{u}_t &= -\epsilon_1(x)\hat{u}_x + c_1(x)\hat{v} + p_1(x)(u(1,t) - \hat{u}(1,t)) && (10.1.1)\\
\hat{v}_t &= \epsilon_2(x)\hat{v}_x + c_2(x)\hat{u} + p_2(x)(u(1,t) - \hat{u}(1,t)) && (10.1.2)\\
\hat{u}(0,t) &= q\hat{v}(0,t) + C\hat{X}(t) && (10.1.3)\\
\hat{v}(1,t) &= U(t) && (10.1.4)\\
\dot{\hat{X}} &= A\hat{X} + e^{Ad_a}L(u(1,t) - \hat{u}(1,t)) && (10.1.5)
\end{aligned}$$

Where $x \in [0,1]$, and the functions $p_1(x)$, $p_2(x)$ and the matrix L are output injection gains. The basic idea of the design is to write out the error dynamics of the system, and later transform the system using a backstepping approach into a stable system. The following transformation is used

$$\begin{aligned}
\tilde{u}(x,t) &= \tilde{\alpha}(x,t) - \int_x^1 P^{uu}(x,\xi)\tilde{\alpha}(\xi,t)d\xi - \int_x^1 P^{uv}(x,\xi)\tilde{\beta}(\xi,t)d\xi && (10.1.6)\\
\tilde{v}(x,t) &= \beta(x,t) - \int_x^1 P^{vu}(x,\xi)\tilde{\alpha}(\xi,t)d\xi - \int_x^1 P^{vv}(x,\xi)\tilde{\beta}(\xi,t)d\xi && (10.1.7)
\end{aligned}$$

Where the tildes denote the errors of their respective variables, and the P variables are the kernels of the transformation. Note that the α and β is not the same as the Riemann invariants used in the simulations. It can be shown that the kernels must satisfy the system of equations

$$\begin{aligned}
\epsilon_1(x)P^{uu}_x(x,\xi) + \epsilon_1(\xi)P^{uu}_\xi(x,\xi) &= -\epsilon_1^{'}(\xi)P^{uu}(x,\xi) + c_1(x)P^{vu}(x,\xi) && (10.1.8)\\
\epsilon_1(x)P^{uv}_x(x,\xi) - \epsilon_2(\xi)P^{uv}_\xi(x,\xi) &= \epsilon_2^{'}(\xi)P^{uv}(x,\xi) + c_1(x)P^{vv}(x,\xi) && (10.1.9)\\
\epsilon_2(x)P^{vu}_x(x,\xi) - \epsilon_1(\xi)P^{vu}_\xi(x,\xi) &= \epsilon_1^{'}(\xi)P^{vu}(x,\xi) - c_2(x)P^{uu}(x,\xi) && (10.1.10)\\
\epsilon_2(x)P^{vv}_x(x,\xi) + \epsilon_2(\xi)P^{vv}_\xi(x,\xi) &= -\epsilon_2^{'}(\xi)P^{vv}(x,\xi) - c_2(x)P^{uv}(x,\xi) && (10.1.11)
\end{aligned}$$

on $\tau_o = \left\{ \ (x,\xi) \ : \ 0 \le x \le \xi \le 1 \ \right\}$, with the boundary conditions

$$\begin{aligned} P^{uu}(0,\xi) &= qP^{vu}(0,\xi) && (10.1.12)\\ P^{uv}(x,x) &= \frac{c_1(x)}{\epsilon_1(x)+\epsilon_2(x)} && (10.1.13)\\ P^{vu}(x,x) &= -\frac{c_2(x)}{\epsilon_1(x)+\epsilon_2(x)} && (10.1.14)\\ P^{vv}(0,\xi) &= \frac{1}{q}P^{uv}(0,\xi) && (10.1.15) \end{aligned}$$

And that we have

$$\begin{aligned} p_1(x) &= Ce^{Ah_\alpha(x)}L - \epsilon_1(1)P^{uu}(x,1) - \int_x^1 P^{uu}(x,\xi)Ce^{Ah_\alpha(\xi)}Ld\xi && (10.1.16)\\ p_2(x) &= -\epsilon_1(1)P^{vu}(x,1) - \int_x^1 P^{vu}(x,\xi)Ce^{Ah_\alpha(\xi)}Ld\xi && (10.1.17) \end{aligned}$$

where $h_\alpha(z) = \int_z^1 \frac{d\gamma}{\epsilon_1(\gamma)}$, and that we must choose L such that (A-LC) is Hurwitz.

10.2 Implementation

It is shown in[4] that the linear model for the MPD rig can be transformed to a system on the form (10.1.1-10.1.5) by the change of coordinates

$$\begin{aligned} u(x,t) &= \frac{1}{2}\left(q(xl,t) + \frac{A}{\rho c}(p(xl,t) - p_{sp} + \rho g l x)\right)\exp(\sigma x) && (10.2.1)\\ v(x,t) &= \frac{1}{2}\left(q(xl,t) - \frac{A}{\rho c}(p(xl,t) - p_{sp} + \rho g l x)\right)\exp(-\sigma x) && (10.2.2) \end{aligned}$$

with

$$\begin{aligned} \epsilon_1(x) &= \epsilon_2(x) = \frac{c}{l} && (10.2.3)\\ c_1(x) &= -\frac{1}{2}\frac{F}{\rho}\exp(2\sigma x) && (10.2.4)\\ c_2(x) &= -\frac{1}{2}\frac{F}{\rho}\exp(-2\sigma x) && (10.2.5)\\ q &= -1, A = \bar{A}, C = -A_2\bar{C} && (10.2.6)\\ \sigma &= \frac{1}{2}\frac{F}{\rho}\frac{l}{c} && (10.2.7) \end{aligned}$$

Note that this model requires knowledge about the frequency of the disturbance, but not the phase and amplitude. For example, a sinusoidal piston disturbance with frequency ω can be modeled as

$$\begin{aligned} \dot{X} &= AX && (10.2.8)\\ v_d(t) &= \bar{C}X && (10.2.9)\\ A &= \begin{bmatrix} 0 & -\omega \\ \omega & 0 \end{bmatrix} && (10.2.10)\\ \bar{C} &= \begin{bmatrix} 0 & 1 \end{bmatrix} && (10.2.11) \end{aligned}$$

Inserting the parameters into the kernel equations, yields the hyperbolic set of PDEs

$$\begin{aligned} P_x^{uu}(x,\xi) + P_\xi^{uu}(x,\xi) &= -\sigma e^{2\sigma x} P^{vu}(x,\xi) && (10.2.12)\\ P_x^{uv}(x,\xi) - P_\xi^{uv}(x,\xi) &= -\sigma e^{-2\sigma x} P^{vv}(x,\xi) && (10.2.13)\\ P_x^{vu}(x,\xi) - P_\xi^{vu}(x,\xi) &= \sigma e^{2\sigma x} P^{uu}(x,\xi) && (10.2.14)\\ P_x^{vv}(x,\xi) + P_\xi^{vv}(x,\xi) &= \sigma e^{-2\sigma x} P^{uv}(x,\xi) && (10.2.15) \end{aligned}$$

on $\tau_o = \left\{ \ (x,\xi) \ : \ 0 \le x \le \xi \le 1 \ \right\}$, with the boundary conditions

$$\begin{aligned} P^{uu}(0,\xi) &= -P^{vu}(0,\xi) && (10.2.16)\\ P^{uv}(x,x) &= -\frac{1}{2}\sigma e^{2\sigma x} && (10.2.17)\\ P^{vu}(x,x) &= \frac{1}{2}\sigma e^{-2\sigma x} && (10.2.18)\\ P^{vv}(0,\xi) &= -P^{uv}(0,\xi) && (10.2.19) \end{aligned}$$

We only need to solve for P^{uu} and P^{vu}, since the others don't appear in the observer gains. The coupled PDEs 10.2.12 and 10.2.14 are solved using the method of characteristics B.1, an outline of the solution algorithm follows.

10.2.1 Solving the Kernel Equations

The set of PDEs 10.2.12 and 10.2.14 have the two characteristic curves B.2

$$\begin{aligned} \frac{dx}{d\xi} &= 1 && (10.2.20)\\ \frac{dx}{d\xi} &= -1 && (10.2.21) \end{aligned}$$

Corresponding to equation 10.2.12 and 10.2.14 respectively. The algorithm proceeds as follows:

1. The values of P^{vu} on the antidiagonal are calculated using the boundary condition 10.2.18.

2. The first value of P^{uu} on the antidiagonal is calculated by using 10.2.16. The rest of P^{uu} on the diagonal is calculated by utilizing that it is a characteristic curve for 10.2.12 (Along the antidiagonal, we have $P^{uu}_x(x,\xi) = -\sigma e^{2\sigma x} P^{vu}(x,\xi)$, and only need to integrate (using Euler's method).

3. The diagonal is a characteristic curve for 10.2.14. Along the diagonal we have $P^{vu}_x(x,\xi) = \sigma e^{2\sigma x} P^{uu}(x,\xi)$. We use Euler's method to calculate the next antidiagonal of values of P^{vu}.

4. We go back to point 2, and repeat until the whole grid is calculated. See figure 10.2.1.

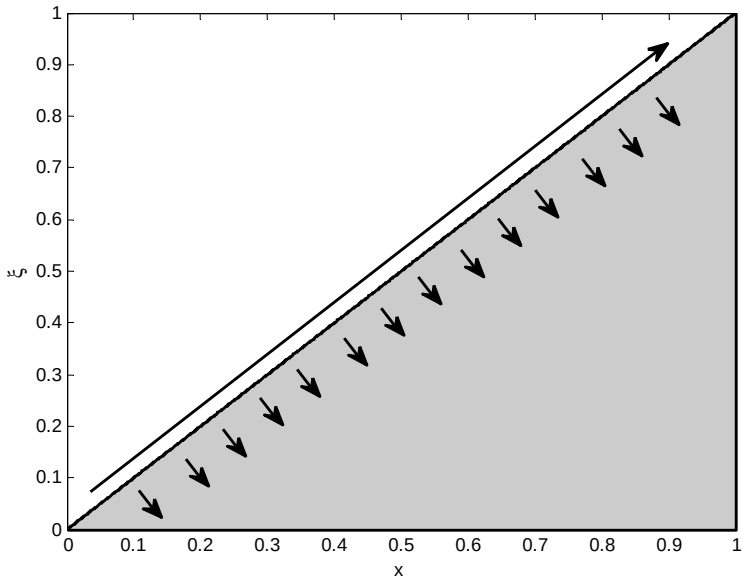

Figure 10.2.1: *The boundary of the kernel equations, and the direction in which we integrate. P^{vu} is first calculated on the antidiagonal. Then the P^{uu} values on the diagonals are calculated.*

After the kernels are calculated, the observer gains are obtained using 10.1.16 and 10.1.17. Notice that the observer gains are functions of the disturbance frequency.

10.2.2 Integration

To implement the observer on the simulator, a few changes had to made since the coordinate system in the simulator (10.2.1, 10.2.2) is slightly different from the Riemann-invariants used in the linear simulator (7.0.6, 7.0.7). Differentiating 10.2.1 and 10.2.2 yields

$$u_t = \frac{1}{2}(q_t + \frac{A}{\rho c}p_t)\exp(\sigma x) \quad (10.2.22)$$

$$v_t = \frac{1}{2}(q_t - \frac{A}{\rho c}p_t)\exp(-\sigma x) \quad (10.2.23)$$

Combined with the derivatives of 7.0.6 and 7.0.7, we get the relations

$$\alpha_t = \frac{2}{A}\exp(-\sigma x)u_t \quad (10.2.24)$$

$$\beta_t = \frac{2}{A}\exp(\sigma x)v_t \quad (10.2.25)$$

Thus, the corrective terms to be implemented in the simulator are

$$\alpha_{t,corr} = \frac{2}{A}\exp(-\sigma x)u_{t,corr} = \frac{2}{A}\exp(-\sigma x)p_1(x)(u(1,t) - \hat{u}(1,t)) \quad (10.2.26)$$

$$\beta_{t,corr} = \frac{2}{A}\exp(\sigma x)v_{t,corr} = \frac{2}{A}\exp(\sigma x)p_2(x)(u(1,t) - \hat{u}(1,t)) \quad (10.2.27)$$

In addition, the corrective term in the disturbance model (10.1.5).

10.2.3 State Vector

The state vector used for the observer contains the same $\alpha-$ and $\beta-$information as the simulator state vector, and two additional states for the disturbance.

10.3 Simulation

Using a disturbance frequency $\omega = \pi/2$, and placing the poles of (A-LC) at $[-40+20i, -40-20i]$ yielded the gain functions $p_1(x)$ and $p_2(x)$ in figure 10.3.1.

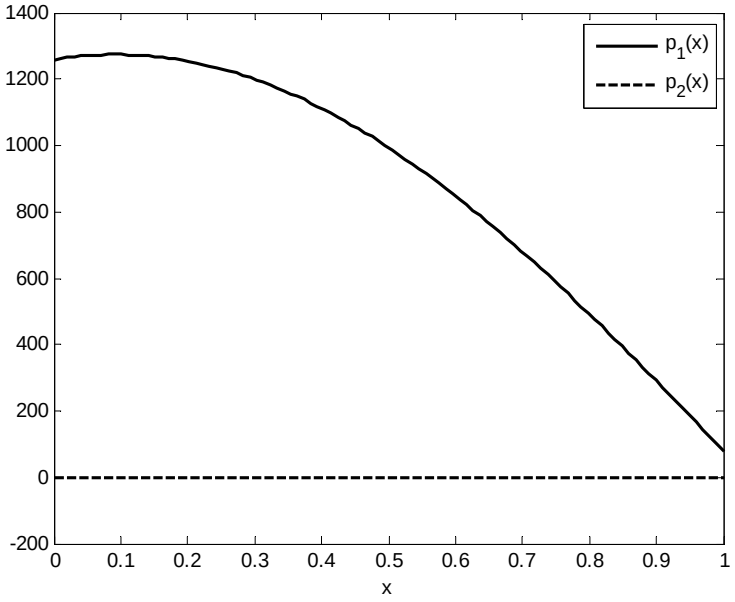

Figure 10.3.1: *Observer gains*

In our case, it turns out that $p_2(x) \approx 0 \forall x$ and $p_1(x) \approx Ce^{Ah_\alpha(x)}L$ (the error of this assumption is in the order 10^{-4}). This is true for all parameters, as long as the friction is small.

A simulation was done, where the topside measurements were fed from the quasi-linear simulator into the linear observer. The simulation time response is shown in figure 10.3.2. As can be seen, the observer converges to the right disturbance and bottom hole pressure (the small discrepancies are thought to be due to the linearization).

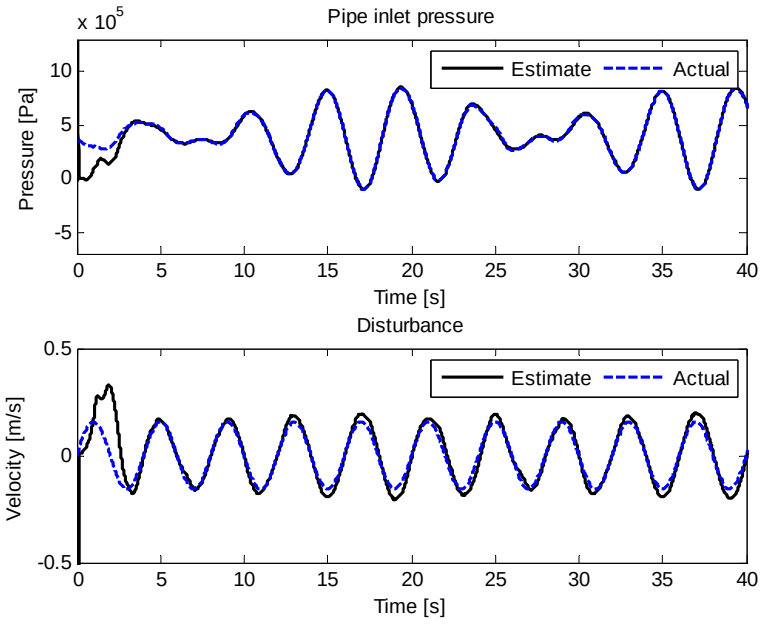

Figure 10.3.2: *Observer time response. Simulated with an initial choke pressure at 4 bar, and the choke varied sinusoidally with a 0.2 Hz frequency and a 0.25 Hz piston disturbance.*

10.4 Lab Test

These are the simulation results from the observer when lab data has been used as the input. First the output when the lab is excited by two sine waves, and the choke opening is kept constant. The data from the lab was gathered with the back pressure pump enabled.

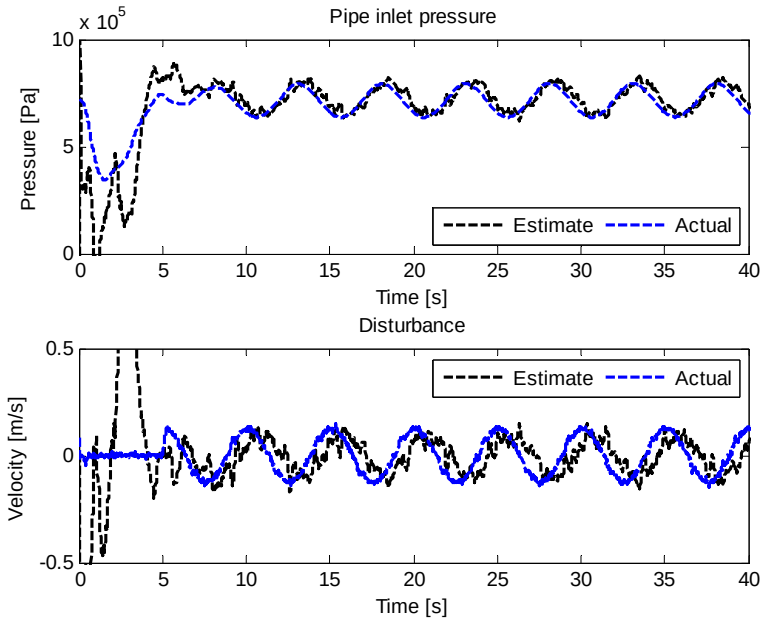

Figure 10.4.1: *Test 1: Observer response with disturbance frequency 0.2 Hz and a choke opening of 45 degrees*

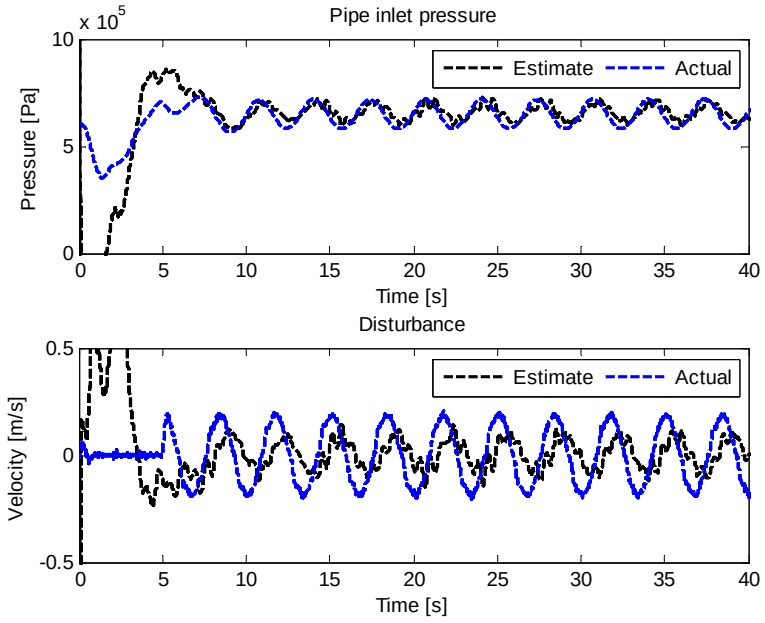

Figure 10.4.2: *Test 2: Observer response with disturbance frequency 0.3 Hz and a choke opening of 50 degrees*

Then a test where both the choke opening and the piston are varied sinusoidally

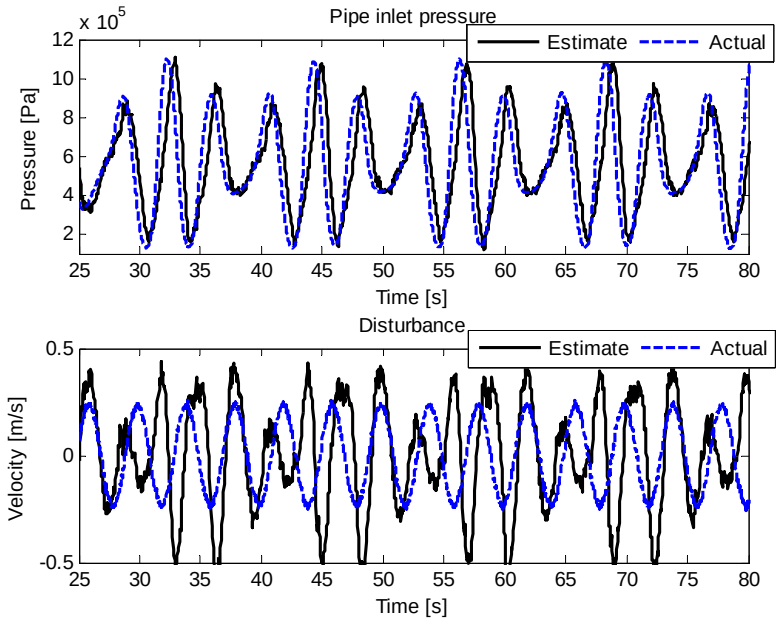

Figure 10.4.3: *Test 3: Observer response with disturbance frequency 0.25 Hz and a choke varying sinusoidally around 53 degrees with a frequency 0.33Hz and a 5 degree amplitude*

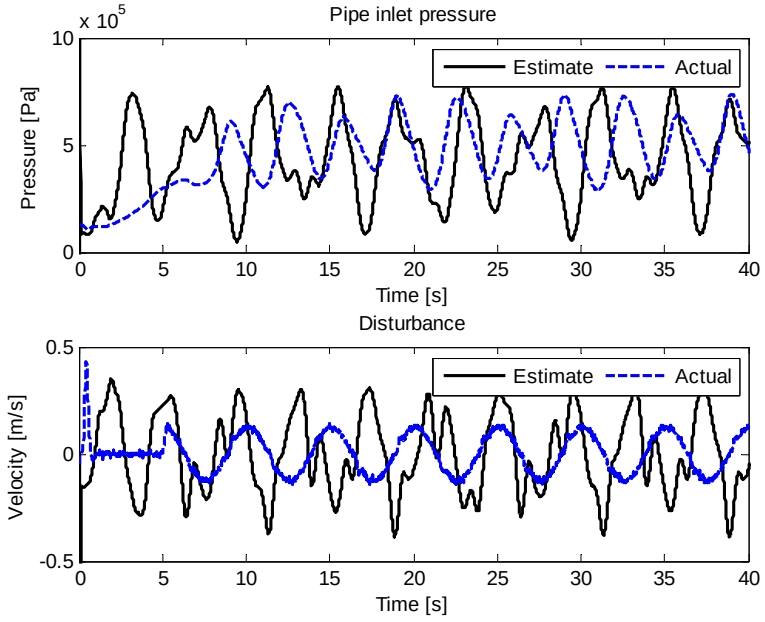

Figure 10.4.4: *Test 4: Observer response with disturbance frequency 0.2 Hz and a choke varying sinusoidally around 40 degrees with a frequency 0.3Hz and a 10 degree amplitude*

As can be seen in the figures, the tracking of the pipe inlet pressure is satisfactory for the

first 3 tests, except that that the estimate is lagging behind the plant by somewhere around 0.3-0.5 seconds. A first thought would be that the wave speed in the observer is wrong, but increasing it made the response worse. A phase shift was also observed in the testing of the simulator, but with the opposite sign. Unlike the simulator, the choke equation is not a part of the observer, which points towards the modeling of the transfer function from the piston disturbance to the system as a contributing cause. Since measurements from the actual piston disturbance flow (FT4) weren't available at the time of this project, it was not possible to verify its dynamics.

Chapter 11 Concluding Discussion and Future Work

When tuning the simulator, some parameters had to be changed significantly from the experimental values. This section summarizes the modeling and the results discovered, and suggestions on future changes in the modeling.

11.1 Copper Pipe

The copper pipe was modeled using the incompressible Navier-Stokes equation with linearized compressibilty. It later turned out that a linear model gave almost exactly the same output, with lower run times.

An interesting phenomenon discovered, was that the speed of sound identified by measuring the transient propagation delay (1173 m/s), did not match the speed of sound corresponding to the resonance frequencies of the system (850 m/s) . This was later confirmed by [7] by experimentally determining the bulk modulus in the system. These observations may indicate that some of the dynamics of the system have been overlooked. Not to mention, the experimentally determined propagation speed corresponds badly to the theoretical value. This may be caused by entrained air or unmodeled elasticity in the system.

When the "topside" rubber tubes are omitted, the resonance peak is moving slightly towards higher frequencies, but not nearly enough to account for the wave speed reduction.

Because of the oscillating nature of the flow in the system, a suggestion is to implement an unsteady friction function and see how this affects the response.

11.2 Choke

The choke was modeled with the steady flow orifice equation. The steady flow assumption proved to be bad at simulating high frequency oscillating flow through the choke, as seen in section 8.4.1. An improvement of the simulator, allowing for faster disturbances, would be including a frequency dependent model for the flow around the choke. Nonetheless, for lower frequencies, the orifice equation seems like a good approximate.

11.3 Piston

The pressure drop over the piston was accuratly modeled by a quadratic polynomial. Yet, the flow from the piston compartment into the copper pipe is not dependent upon the pressure drop at the present moment, which is only used to calculate the additional pressure difference from the pipe inlet to the bottom. The flow generated using this assumption is identical to the flow from a model accounting for compressibility (the compressibility effects don't seem to affect the response much in such a small volume). As future work, the dynamics around the piston should be looked into as soon as the pipe inlet flow meter is in place. There might be some additional compressibility due to the elasticity of the compartment itself and the rubber hose going from the piston compartment and into the copper pipe that may add a time delay.

11.4 Pump

The pump is currently modeled as a static relation between the setpoint and the outlet pressure, based on data obtained by pressurizing the system. Results from [24] indicate that the frequency response of the system is significantly different when the back pressure pump is enabled, with lower resonance peaks for lower frequencies.

11.5 Range of Validity

The frequency response of the simulator indicates that roughly, the prediction of the bottom hole pressure, given a choke opening, a pump setting and a disturbance, is approximated well for all disturbance frequencies up to the first resonance peak (0.44Hz for closed choke, 0.25Hz for open choke). The prediction of the states around the choke seem to be deteriorating a little earlier.

A limitation of the model is that it may produce negative pressures in the system. If this poses a problem, it may be avoided by increasing the choke outlet pressure.

The observer seems to produce good estimates of the bottom hole pressure in approximately the same range as the simulator. The response is slightly lagging, which may indicate unmodelled dynamics in the copper pipe. But the results overall are promising for future model-based control of the lab rig. First, the robustness of the observer should be further examined and improved.

Chapter A User Guide - Getting Started

A.1 Package Contents

The files enclosed with this report includes a linear simulator, a quasi-linear simulator and an observer, organized in a Simulink library. In addition, scripts for calculating the observer gains and the frequency response of the system are enclosed, as well as a logging and plotting tool that produces an animated version of the pressure data. The source code for the version of the simulator with the piston model 5.4.1 is also included. Remember that this model uses different friction parameters for the choke (about 3000 and 9000 for the linear and quadratic term respectively)

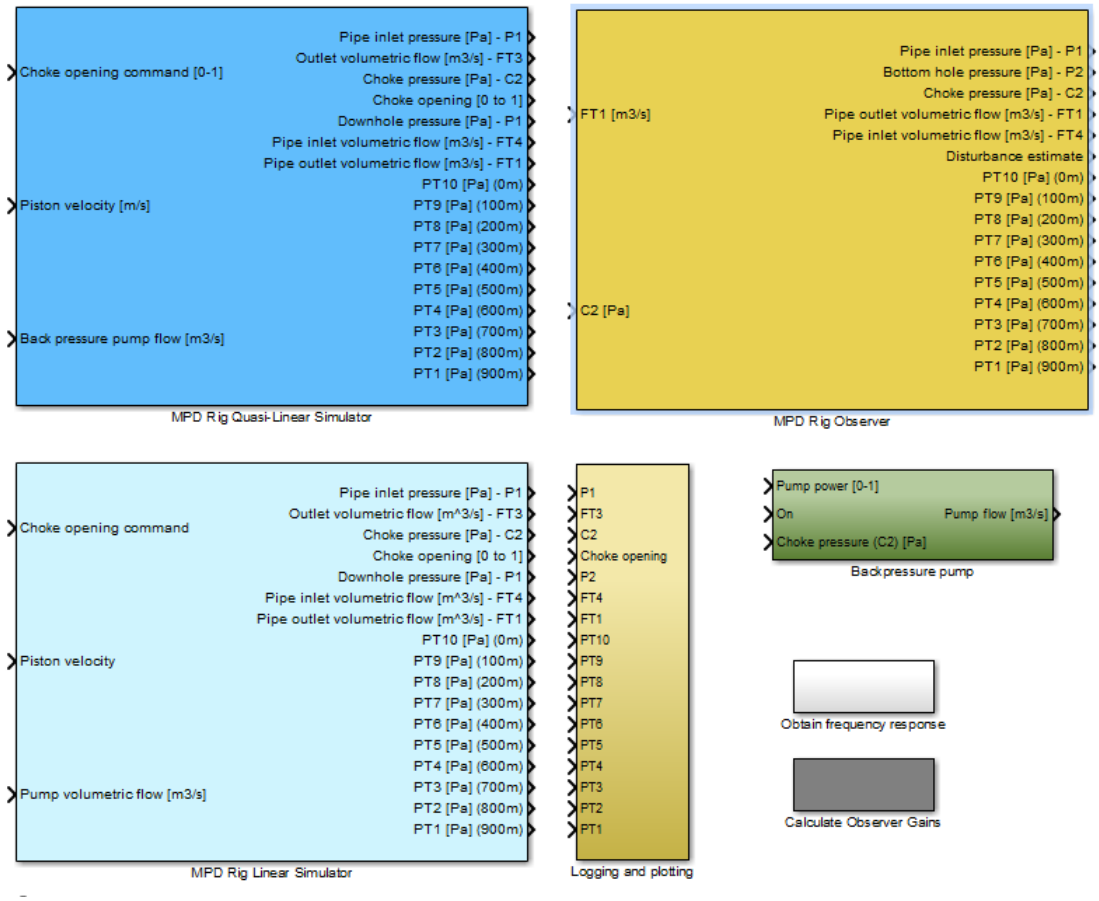

Figure A.1.1: *Library contents*

A.2 Get Started with the Simulator

MATLAB R2012 or newer is required to run the simulator.

Start by creating a new Simulink file. Open the library (MPDHeaveLib.slx) and drag one of the simulator blocks into your new Simulink file.

There are basically 3 things that should be configured before running the simulator.

1. The choke opening needs to be set to a number between 0 and 1.
2. The piston reference in m/s
3. The pump flow in m^3/s

In addition, the initial outlet pressure and the initial choke pressure can be adjusted in the parameter list in the Simulator block. The initial choke pressure needs to be larger than the outlet pressure, otherwise the simulator will crash.

The block "Logging and plotting" takes care of all the logging. Double click to see the MATLAB workspace variable names corresponding to the different measurements. An animated pressure plot may be enabled by uncommenting the subsystem "Pressure plot".

Note that the pressures in the simulator are absolute pressures. The pressure values from the lab are gauge pressures.

A.3 Adjusting Default Parameter Values

To adjust the default values, the library has to be unlocked (Diagram->Unlock Library).

A.4 Get Started with the Observer

Start by creating a new Simulink file. Drag an observer block from the library into the new file. Make sure the working directory of MATLAB is the library root folder. Double click on the observer to specify the outlet pressure and the disturbance frequency. Go to the library and double click on "Calculate Observer Gains", or open the file obsgains.m. Specify the disturbance frequency and run the file. You are now good to go. Remember, the pressures from the lab are gauge pressures, and in different units.

A.5 How to...

A.5.1 Customize Pressure Outputs

Change the vector "Desired pressure outputs (m)" in the parameter list to automatically change the pressure outputs. This can be done for the simulators as well as the observer.

A.5.2 Recompile the Code

If changes are made to the source code, it needs to be recompiled using the command "mex FILENAME". This requires a supported compiler. See the MATLAB manual for details. When the source code is compiled, replace the old .mexw64-file with the new one.

A.5.3 Change the Number of Discretization Elements

Change the constant C_N in the source code and recompile. This was implemented as a constant since the number of states in the system needs to be known before the simulation starts.

A.5.4 Obtain the Frequency Response

Double-click on the box named "Obtain frequency response" to simulate and get the frequency response from the piston position to the bottomhole pressure.

A.6 On Solvers

Recommended solvers to be used on simulations include ode8 (Dormand-Prince) with a fixed step length 0.01 and ode45. Some of the lower-order fixed-step solvers require shorter step lengths to be stable.

Chapter B Mathematical background

B.1 Method of Characteristics

The method of characteristics is a technique for solving hyperbolic partial differential equations. Consider the first order equation

$$\mathrm{z_t} + \mathrm{az_x} = 0 \tag{B.1.1}$$

The solution along the curve $x(t) = x_0 + at$ can be investigated by differentiating z along this line

$$\frac{d}{dt}z(x(t),t) = \frac{\partial}{\partial t}z(x(t),t) + \frac{\partial}{\partial x}z(x(t),t)x'(t) = z_t + az_x = 0 \tag{B.1.2}$$

Thus, the value of z does not change along this line. The same can be shown along the other characteristic curve of B.1.1. Consider now the system

$$\mathrm{z_t} + \mathrm{az_x} = f(z,x,t) \tag{B.1.3}$$

Again, the solution along the curve $x(t) = x_0 + at$ can be investigated:

$$\frac{d}{dt}z(x(t),t) = \frac{\partial}{\partial t}z(x(t),t) + \frac{\partial}{\partial x}z(x(t),t)x'(t) = z_t + az_x = f(z,x,t) \tag{B.1.4}$$

So along the characteristic curves, we get the ordinary differential equation

$$\frac{dz}{dt} = f(z,x,t) \tag{B.1.5}$$

If an initial solution z_0 is known, we only need to integrate the right hand side with respect to time to get the solutions along the characterstic curve. If this is done for several initial values, we can make a grid of characteristic curves, and get the solutions for a grid of (x,t)-values. This method is also generalizable to higher order systems.

B.2 Riemann Invariants

We can gain insight and possibly explicit solutions of systems of first order PDEs on the form $\mathbf{z_t} + \mathbf{A(z)z_x} = 0$ by using the concept of Riemann invariants ([21] p. 336). A system on this form is considered strictly hyperbolic if the eigenvalues $\lambda^{(i)}$ of the matrix A(z) are distinct and real. Consider the definition of the left eigenvectors $\mathbf{l}^{(i)}$ for a system of 2 PDEs

$$\mathbf{l}^{(i)}(\mathbf{I}\lambda^{(i)} - \mathbf{A}) = \mathbf{0}, \text{ for i=1,2} \tag{B.2.1}$$

If we premultiply the PDE by its generalized left eigenvector ($\mathbf{l}^{(i)}$) and insert (B.2.1), we obtain

$$\mathbf{l}^{(i)}(\mathbf{z}_t + \lambda^{(i)}\mathbf{z}_x) = 0, \text{ for i=1,2} \tag{B.2.2}$$

The bracketed term in (B.2.2) is the directional derivative of $\mathbf{z}$ with respect to time along the family of characteristic curves $C^{(i)}$ defined by

$$C^{(i)} : \frac{dx}{dt} = \lambda^{(i)}, \text{ for i=1,2} \tag{B.2.3}$$

If we denote differentiation with respect to time along the $C^{(1)}$ family of characteristics by $d/d\sigma_1$ and along the $C^{(2)}$ family of characteristics by $d/d\sigma_2$ (B.2.2) becomes

$$\mathbf{l}^{(1)}\frac{d\mathbf{z}}{d\sigma_1} = 0 \tag{B.2.4}$$

and along the $C^{(2)}$ family of characteristics

$$\mathbf{l}^{(2)}\frac{d\mathbf{z}}{d\sigma_2} = 0 \tag{B.2.5}$$

By multiplying the equations (B.2.4) and (B.2.5) by appropriate integrating factors μ_1 and μ_2 we obtain along the $C^{(1)}$ and $C^{(2)}$ characteristics respectively

$$\alpha(z_1, z_2) = \int \mu_1 l_1^{(1)} dz_1 + \int \mu_1 l_2^{(1)} dz_2 \tag{B.2.6}$$

$$\beta(z_1, z_2) = \int \mu_2 l_1^{(2)} dz_1 + \int \mu_2 l_2^{(2)} dz_2 \tag{B.2.7}$$

where α and β are called Riemann invariants of the system, and $\mathbf{l}^{(i)} = \begin{bmatrix} l_1^{(i)} & l_2^{(i)} \end{bmatrix}$. The Riemann invariants are constant along the $C^{(1)}$ and $C^{(2)}$ characteristics. Each Riemann invariant can be looked at as the "information" that travels along the characteristic line in x-t-space. We will use this to ease implementation of the PDE governing the pipe flow.

Chapter C Simulink I/O

Channel	Unit	Sensor
2	P2	Druck PTX 1400
3	P1	Druck PTX 1400
4	C2	Druck UNIK 5000 PS
5	C1	Druck UNIK 5000 PS
6	PT1	Druck UNIK 5000 PS
7	Tank water level	Druck PTX 1400
8	PT8	Druck UNIK 5000 PS
9	PT6	Druck UNIK 5000 PS
10	PT9	Druck UNIK 5000 PS
11	PT2	Druck UNIK 5000 PS
12	PT3	Druck UNIK 5000 PS
13	PT7	Druck UNIK 5000 PS
14	PT4	Druck UNIK 5000 PS
15	PT10	Druck UNIK 5000 PS
16	PT5	Druck UNIK 5000 PS
18	FT1	Heinrichs EP/UMF2
19	FT3	Parker DFT990
20	FT2	Parker DFT990
21	FT4	Not delivered yet
27	FT1 sign bit	
31	Pulse generator position feedback	
32	Choke position feedback	

Table C.0.1: *Analog input channels in Simulink*

Channel	Unit	Range
1	Choke angle	0-10 V
2	Heave generator/piston position	0-10 V

Table C.0.2: *Analog output channels*

Bibliography

[1] *Study of Fluid Transients in Closed Conduits*. Oklahoma State University.

[2] Managed pressure drilling, 2007. By Weatherford.

[3] Ole Morten Aamo. A dynamic model of the ipt heave lab.

[4] Ole Morten Aamo. Disturbance rejection in 2x2 linear hyperbolic systems. *IEEE Transactions on Automatic Control*, 2012.

[5] Anton Bergant, Angus Ross Simpson, and John Vitkovsky. Developments in unsteady pipe flow friction modelling. *Journal of Hydraulic Research*, 39:249–257, 2001.

[6] Andreas Boge. Experimental work and modeling of surge and swab effects. Master's thesis, NTNU, 2012.

[7] Andreas Boge. (untitled as of june 10) master thesis 2013. Master's thesis, NTNU, 2013.

[8] Karen Bybee. Compensation of surge and swab pressures in floating drilling operations. *Journal of Petroleum Technology*, February:52–54, 2008.

[9] Robert Drønnen. Disturbance attenuation in managed pressure drilling: Mimicking heave-like disturbance in an experimental lab setup. Master's thesis, NTNU, 2012.

[10] H.-F. Duan, M. S. Ghidaoui, P. J. Lee, and Y. K. Tung. Relevance of unsteady friction to pipe size and length in pipe fluid transients. *Journal of Hydraulic Engineering*, 138:154–166, 2012.

[11] Olav Egeland and Jan Tommy Gravdahl. *Modeling and Simulation for Automatic Control*. Marine Cybernetics, 2003.

[12] Dave Elliott, Julio Montilva, Paul Francis, Don Reitsma, Jaye Shelton, and Vincent Roes. Managed pressure drilling erases the lines. *Oilfield Review*, 23:14–23, 2011.

[13] Philip Frink. Managed pressure drilling - what is in a name? *Drilling Contractor*, March/April:36–39, 2006.

[14] Deepak M. Gala and Julmar Shaun Toralde. Managed pressure drilling 101: Moving beyond "it's always been done that way". *The Way Ahead*, 7:12–14, 2011.

[15] Camilla Sunde Gjengseth. Lab for heave motion during managed pressure drilling. Master's thesis, NTNU, 2012.

[16] Martin Standal Gleditsch. Mimicking heave-like disturbances for managed pressure drilling using an experimental lab setup. Master's thesis, NTNU, 2012.

[17] John-Morten Godhavn and Kjetil Arne Knudsen. High performance and reliability for mpd control system ensured by extensive testing. 2010.

[18] John-Morten Godhavn, Alexey Pavlov, Glenn-Ole Kaasa, and Nils Lennart Rolland. Drilling seeking automatic control solutions. 2011.

[19] Don Hannegan. Offshore drilling hazard mitigation: Controlled pressure drilling redefines what is drillable. *Drilling Contractor*, January/February:84–89, 2009.

[20] Steve Jacob and John Donnelly. Crossing the technology chasm: Managed pressure drilling. *Journal of Petroleum T*, February:30–34, 2011.

[21] Alan Jeffrey. *Applied Partial Differential Equations - An Introduction*. Academic Press, 2003.

[22] Changjun Li, Kexi Liao, Wenlong Jia, and Xia Wu. Waterhammer analysis of oil transportation pipeline using brunone-vitkovsky unsteady flow friction model. In *Power and Energy Engineering Conference (APPEEC), 2011 Asia-Pacific*, pages 1–5, 2011.

[23] Shijie Liu, Artin Afacan, Hisham A. Nasr-El-Din, and Jacob H. Masliyah. An experimental study of pressure drop in helical pipes. *Proceedings: Mathematical and Physical Sciences*, 444:307–316, 1994.

[24] Mart. Disturbance attenuation in managed pressure drilling using impedance matching and an experimental lab setup. Master's thesis, NTNU, 2013.

[25] George H. Medley and Patrick B. B. Reynolds. Distinct variations of managed pressure drilling exhibit application potential. *World Oil*, 227, 2006.

[26] Ken Muir. Mpd techniques address problems in drilling southeast asia's fractured carbonate structures. *Drilling Contractor*, Nov/Des:34–36, 2006.

[27] Jussi Mikael Ånestad. Disturbance attenuation in managed pressure drilling: Tracking control of the choke pressure. Master's thesis, NTNU, 2012.

[28] A. O. Nieckele, A. M. B. Braga, and L. F. A. Azevedo. Transient pig motion through gas and liquid pipelines. *Journal of Energy Resources Technology*, 123:260–269, 2001.

[29] Tollef-Ingebret Svenum. Lab for heave motion during managed pressure drilling. Master's thesis, NTNU, 2012.

[30] Philip J Thomas. *Simulation of Industrial Processes for Control Engineers*. Butterworth-Heinemann, 1999.

[31] E. Benjamin Wylie and Victor L. Streeter. *Fluid Transients*. McGraw-Hill, 1978.